iScience

CellPress

Article

G-quadruplex Structures Contribute to Differential Radiosensitivity of the Human Genome

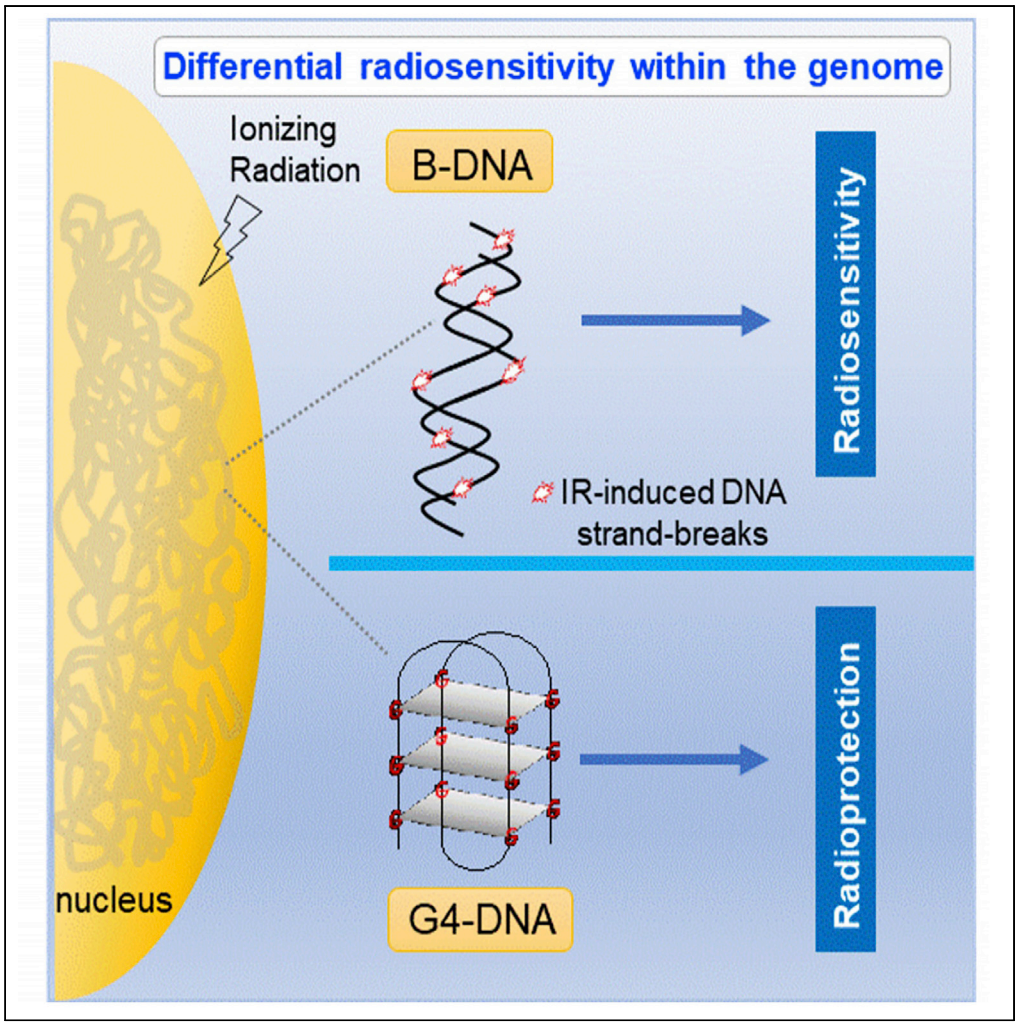

Nitu Kumari, Supriya V. Vartak, Sumedha Dahal, ..., Vidya Gopalakrishnan, Bibha Choudhary, Sathees C. Raghavan

sathees@iisc.ac.in

HIGHLIGHTS

G4 DNA contributes to genome-wide radioprotection and is modulated by G4 resolvases

Radiation causes minimal damage at the G4 structures at telomeres

Formation of G4 DNA contributes toward differential radiosensitivity of human genome

Planar quartet of G4 DNA is shielded from IR-induced free radicals and thus DNA breaks

Kumari et al., iScience 21, 288–307
November 22, 2019
https://doi.org/10.1016/j.isci.2019.10.033

iScience

CellPress

Article

G-quadruplex Structures Contribute to Differential Radiosensitivity of the Human Genome

Nitu Kumari,[1,5] Supriya V. Vartak,[1,5] Sumedha Dahal,[1,5] Susmita Kumari,[1,6] Sagar S. Desai,[2,3,6] Vidya Gopalakrishnan,[1,4,6] Bibha Choudhary,[2] and Sathees C. Raghavan[1,7,*]

SUMMARY

DNA, the fundamental unit of human cell, generally exists in Watson-Crick base-paired B-DNA form. Often, DNA folds into non-B forms, such as four-stranded G-quadruplexes. It is generally believed that ionizing radiation (IR) induces DNA strand-breaks in a random manner. Here, we show that regions of DNA enriched in G-quadruplex structures are less sensitive to IR compared with B-DNA *in vitro* and inside cells. Planar G-quartet of G4-DNA is shielded from IR-induced free radicals, unlike single- and double-stranded DNA. Whole-genome sequence analysis and real-time PCR reveal that genomic regions abundant in G4-DNA are protected from radiation-induced breaks and can be modulated by G4 stabilizers. Thus, our results reveal that formation of G4 structures contribute toward differential radiosensitivity of the human genome.

INTRODUCTION

Maintaining genomic stability is of utmost importance for survival of any organism. Our genome is constantly challenged by a number of endogenous and exogenous insults, and studies estimate ~1000 DNA lesions in each cell per day (Aguilera and Garcia-Muse, 2013; Burma et al., 2006; Ciccia and Elledge, 2010). Endogenous sources comprise of free radicals generated during metabolic processes, DNA replication, and recombination, whereas the exogenous agents include radiation and DNA-damaging chemicals. Among exogenous agents, radiation is the most significant contributor to DNA damage. Ultraviolet rays (UV), ionizing radiations (IR; X-rays, γ-rays), microwaves etc. are examples of radiations that cause an array of ill effects in cells. Although UV radiation is highly pervasive and causes DNA lesions such as cyclobutane pyrimidine dimers (CPDs) and single-strand breaks (SSBs), majority of DNA damage caused by IR results in SSBs and double-strand breaks (DSBs) (Vignard et al., 2013).

IR damages DNA either directly, wherein DNA breaks occur due to transfer of energy to the phosphodiester bonds, or indirectly by initiating radiolysis of water molecules present in close vicinity of the DNA, subsequently resulting in the production of free radicals. Upon induction of an SSB or DSB, the affected cell manifests a cascade of events, collectively termed as the DNA damage response (DDR), which includes sensing of the DSBs, transduction of the sensed signal, and activation of repair factors, ultimately ensuring the genomic integrity and hence, an intact chromosome. The degree and type of DNA damage dictates whether a cell survives (DNA repair) or undergoes apoptosis (Jackson and Bartek, 2009; Sancar et al., 2004; Symington and Gautier, 2011).

Two schools of thought exist regarding distribution of IR-induced DNA strand-breaks within the genome (Lobrich et al., 1996; Pang et al., 2005; Vignard et al., 2013). Most studies indicate that radiation-induced breaks are random, occur throughout the genome and do not follow a pattern (Lett, 1992; Nikiforov et al., 1999; Pang et al., 2005; Van Der Schans, 1978). On the other hand, a few studies indicate nonrandom pattern of IR-induced DNA strand-breaks (Lobrich et al., 1996; Zhou et al., 2012). It is reported that the four nucleotide bases (adenine, cytosine, guanine, and thymine) vary in their sensitivity to IR-induced DNA damage, guanine being the most readily oxidized among the four (Spotheim-Maurizot and Davidkova, 2011; Steenken, 1997). However, whether this contributes to differential sensitivity of DNA to IR is not clear. Moreover, its implication with respect to the genome remains unexplored.

Organisms differ in the degree of sensitivity to IR-induced DNA damage. This property is attributed to a number of factors such as complexity of genome of the organism, cellular organization, variation in the DNA damage

[1]Department of Biochemistry, Indian Institute of Science, Bangalore 560012, India

[2]Institute of Bioinformatics and Applied Biotechnology, Electronics City, Bangalore 560100, India

[3]Manipal Academy of Higher Education, Manipal, Karnataka, 576104, India

[4]Department of Zoology, St. Joseph's College, Irinjalakkuda, Kerala, 680121, India

[5]These authors contributed equally

[6]These authors contributed equally

[7]Lead Contact

*Correspondence: sathees@iisc.ac.in

https://doi.org/10.1016/j.isci.2019.10.033

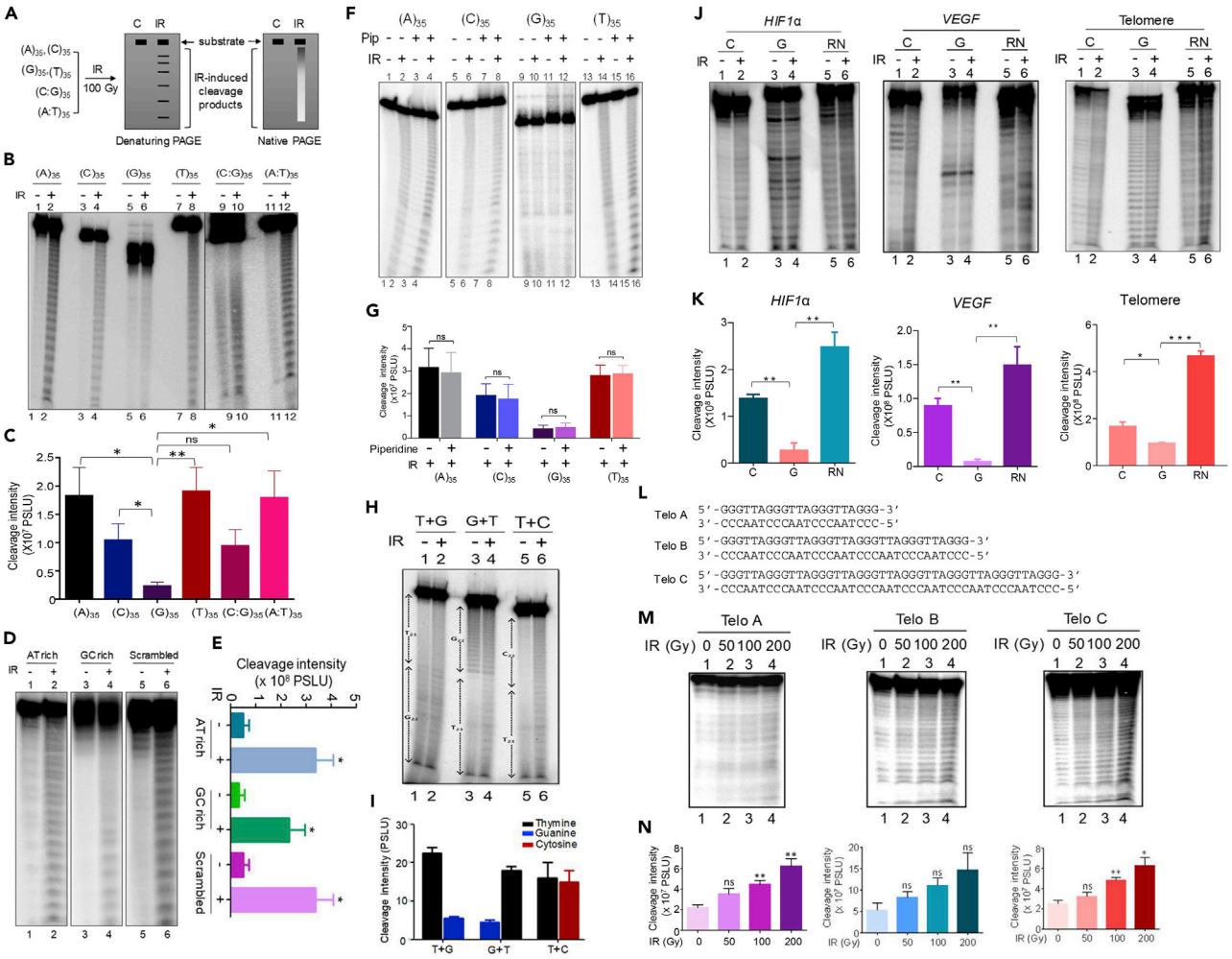

Figure 1. Evaluation of Radiation Sensitivity on Shorter DNA Fragments when Different Sequences or Structures Are Present

(A) Schematic representation of the assay used for evaluation of IR-induced DNA strand-breaks. Oligomeric DNA substrates of interest were γ-irradiated (100 Gy), resolved on a denaturing (observed as a ladder) or native gel (observed as a smear), and analyzed for the abundance of DNA breaks using PAGE.

(B) Denaturing PAGE profile showing sensitivity of single-stranded homopolymeric (35 mer) adenine, cytosine, guanine, and thymine nucleotides and double-stranded DNA ($[A:T]_{35}$ and $[C:G]_{35}$), to γ-radiation (100 Gy).

(C) Bar graph presented shows quantitation of cleavage efficiency for DNA substrates following irradiation. Each experiment was performed a minimum of three times and the intensity of quantified bands is expressed as photo-stimulated luminescence units (PSLU), showing mean ± SEM (*$p < 0.05$, **$p < 0.01$, ***$p < 0.001$).

(D and E) Denaturing PAGE profile showing sensitivity of AT-rich, GC-rich, and scrambled double-stranded (35 mer) DNA to γ-radiation (100 Gy) (D) and bar diagram representing its quantitation (n = 3) showing mean ± SEM (*$p < 0.05$, **$p < 0.01$, ***$p < 0.001$) (E).

(F) Denaturing PAGE profile showing the effect of piperidine treatment on irradiated homopolymeric A, C, G, and transfer DNA sequences. In each case, DNA substrates were irradiated (100 Gy), treated with piperidine (1:10 dilution; 90°C for 30 min), followed by resolving on a 15% denaturing PAGE. "Pip" refers to piperidine treatment. The experiment was repeated multiple times (n = 6).

(G) Bar diagram represents IR-induced cleavage intensity based on panel F and other gels (n = 6) showing mean ± SEM (*$p < 0.05$, **$p < 0.01$, ***$p < 0.001$, "ns" is nonsignificant).

(H) PAGE profile showing radiation sensitivity in three independent heteropolymeric DNA substrates (T23G22, G22T23, and T23C22). Dotted arrow lines indicate position of G, C, or T in the respective DNA.

(I) The intensity of cleaved products was quantified and presented as a bar graph (n = 3) showing mean ± SEM.

(J) PAGE profiles of oligomeric DNA harboring G4-forming motifs (indicated as "G") derived from *HIF1α* promoter, *VEGF* promoter, human telomere sequence upon irradiation (150 Gy). Irradiated complementary strands (marked as "C") derived from same genes and their corresponding random sequence (marked as "RN") served as controls. Experiments were repeated a minimum of three times.

(K) Bar graph showing efficiency of IR-induced cleavage shown in panel J and other gels. In each case, the intensity of IR-induced cleavage was determined following subtraction of background from respective unirradiated control and graph depicts mean ± SEM (*$p < 0.05$, **$p < 0.01$, ***$p < 0.001$).

Figure 1. *Continued*

(L–N) Comparison of IR-induced breaks on double-stranded oligomers derived from three different regions of telomeric DNA (L) named as "Telo A" (3 repeats), "Telo B" (5 repeats), and "Telo C" (7 repeats). PAGE profile shows comparison of cleavage efficiency when increasing dose of IR (0, 50, 100, 200 Gy) was used (M). Bar diagram showing quantification of IR-induced cleavage on duplex DNA containing telomeric repeats is presented (n = 3). Bar graph showing mean ± SEM (*p < 0.05, **p < 0.01, ***p < 0.001, "ns" is nonsignificant) (N).
See also Figure S1.

sensing, and repair mechanisms (Daly, 2009). For example, the bacterium *Deinococcus radiodurans* is extremely resistant to IR-induced DNA damage, whereas other species within the same genus exhibit IR sensitivity (Krisko and Radman, 2013). Interestingly, among the reasons attributed to radiation resistance, skewed GC content forms an important factor, wherein radiation-resistant organisms such as *D. radiodurans* (66.6%) and *Kineococcus radiotolerans* (74.2%) possess higher GC content compared with the susceptible ones such as *Escherichia coli* (50%) or *Shewanella oneidensis* (45.9%). Discrepancy in radiation sensitivity has also been reported among chromosomes, with some chromosomes affected more often than others, although the reasons behind it remain elusive. Interestingly, distinct clusters of DNA damage, often termed as damage "hot spots," within the same chromosome have been reported, suggesting variations in radiation sensitivity among genomic regions (Puerto et al., 2001). Although factors such as GC content and chromatin organization were speculated to be responsible for the difference, the mechanistic details remain unexplored.

The human genome, containing 3000 megabases, has a GC content of 42% and largely exists in the form of B-DNA. However, the last decade has witnessed increasing evidence for the formation and regulation of deviant structures, termed as "non-B DNA" forms inside cells (Sinden, 1994). Structures such as G-quadruplex, triplex DNA, R-loops, cruciforms, and Z-DNA have been shown to play key roles in governing several physiological and pathological processes within a cell, such as transcription, replication, telomere maintenance, and generation of chromosomal translocations (Nambiar et al., 2008, 2011; Nambiar and Raghavan, 2011; Neidle and Balasubramanian, 2006; Raghavan et al., 2004; Sinden, 1994; Voloshin et al., 1988). G-quadruplex (G4-DNA) is formed in guanine-rich regions of DNA and RNA in the cell (Nambiar et al., 2008; Neidle and Balasubramanian, 2006; Sinden, 1994). It typically consists of four three-guanine repeats, held together by Hoogsteen-hydrogen bonding. The guanines form a planar quartet structure, stabilized by monovalent cations such as K^+ that are present in the cellular milieu. Studies have shown several G4-forming motifs (350,000 to 700,000) present throughout the genome in regions including promoters, immunoglobulin switch regions, rDNA, telomeres, and replication origin of several genes (Chambers et al., 2015; Nambiar and Raghavan, 2011). Apart from regulating normal cellular processes, G-quadruplexes have also been implicated in deregulation of oncogenes, tumor suppressors, generation of chromosomal translocations, and hence, oncogenesis (Nambiar and Raghavan, 2011). Thus, whether the human genome is differentially susceptible to radiation-induced DNA damage and if so, the cause behind such a disparity, its mechanism, and relevance is not well understood.

In the present study, we report formation of G-quadruplex DNA structure as an important factor contributing to differential radiosensitivity of genome in human cells. Further, our study establishes that G-quadruplex structures are shielded from radiation-induced DNA breaks *in vitro*, *ex vivo*, and *in vivo*. Thus, our study demonstrates a nonrandom pattern of IR-induced DNA breaks within the human genome due to free radical shielding by DNA G-quadruplex structures.

RESULTS

Homopolymeric Guanine Tracts Harbor Minimal DNA Strand-Breaks upon IR Exposure

Efficiency of radiation-induced cleavage on short DNA was investigated by irradiating single-stranded homopolymeric DNA harboring adenine (A), cytosine (C), guanine (G), and thymine (T) nucleotides (Figure 1A). Irradiation using IR (γ-rays) and subsequent DNA damage leading to DNA breaks was analyzed on a denaturing PAGE (Figure 1B). Results showed significant breakage of DNA on every nucleotide in case of single-stranded polyadenine, polycytosine, and polythymine DNA (Figure 1B). To our surprise, DNA with polyguanine exhibited minimal cleavage upon irradiation, and the intensity of cleavage was comparable with that of the unirradiated control (Figures 1B and 1C). Similar results were also observed when irradiated samples were loaded on a native PAGE (Figures S1A and S1B). We chose a relatively higher dose (100 Gy) to ensure breakage at every nucleotide. A dose-dependent increase in cleavage efficiency was observed when the homopolymeric DNA containing A, C, and T were irradiated with increasing doses of IR (Figure S1C). Consistent to above observation, shielding effect was observed for the G-rich sequence

even after a broad-range dose titration (Figures S1C and S1D). Importantly, as expected, IR-induced breaks were random leading to breakage at almost every nucleotide when double-stranded DNA containing poly C:G or poly A:T were used (Figure 1B). Similar results were also obtained when oligomers containing AT-rich, GC-rich, or scrambled double-stranded DNA sequences were used (Figures 1D and 1E). Besides generation of DNA breaks, exposure to IR also can result in oxidative damage to individual bases (Cadet and Wagner, 2013; Pouget et al., 2002). To assess whether the polyG DNA under investigation was undergoing IR-mediated oxidative damage, homopolymeric oligomers (A, C, G, and T) were irradiated, followed by piperidine treatment, which can convert a base damage into a strand-break and were subsequently resolved on a denaturing PAGE (Figure 1F). Results revealed that IR-induced cleavage on polyG substrate was significantly less, as compared with other homopolymers, even in the presence of piperidine (Figures 1F and 1G). Importantly, there was no significant difference in induction of strand-breaks even upon piperidine treatment in polyG oligomer, thus ruling out the possibility of extensive base damage in this substrate. Multiple bands observed in case of the polyG oligomer, running lower to those of poly A, C, and T is due to formation of intramolecular G-quadruplexes (Figures 1B, S1A, and S1C).

In order to investigate whether the reduced sensitivity observed on homopolymers of guanines was consistent even in the case of heteropolymeric DNA substrates, we designed oligomers harboring guanine-repeat tracts, in combination with other sequences. Interestingly, IR-induced DNA breaks were consistently observed specifically at the poly thymine end of the oligomer, sparing the end containing guanines, whereas the control oligomer (containing thymines and cytosines) harbored breaks throughout its length (Figures 1H and 1I). In some of the guanine-containing oligomers, we consistently found an elevated inherent level of cleavage, when compared with oligomers with other nucleotide sequences. This could be due to the highest oxidation potential of guanines among the 4 nucleotides (Spotheim-Maurizot and Davidkova, 2011; Steenken and Jovanovic, 1997). However, radiation-induced cleavage observed in the other three polynucleotides was always over and above the basal one, unlike in the case of G-rich oligomer. Normalization of the IR-induced cleavage intensity with that of the basal cleavage for respective oligomers revealed a distinct difference between G-rich and other nucleotide sequences.

The polyguanine sequences can fold into non-B DNA, G4 structures owing to the Hoogsteen hydrogen bonding between the four G residues; in addition to the typical Watson-Crick base pairing, it may have at the loop regions (Bochman et al., 2012; Mirkin, 2013; Nambiar et al., 2011; Sinden, 1994). In order to investigate the G4 structure-forming ability of the polyguanine tracts under study, the G-rich oligomer was subjected to circular dichroism (CD) analyses (Figures S1E and S1F). Results revealed that the guanine homopolymers folded into a parallel G-quadruplex, resulting in a typical absorption spectrum with a peak at 260 nm and a trough at 240 nm, as opposed to the C-rich and duplex C:G-rich controls (Figure S1E) (Nambiar et al., 2013; Neidle and Balasubramanian, 2006). Further, gel mobility shift assay results showed that the G-rich oligomer could fold into an intramolecular (faster migrating species as compared with the corresponding cytosine control), and an intermolecular G-quadruplex (slower migrating species), as compared with its C counterpart (Figure S1A, lanes 5,6). Moreover, CD studies revealed that the G-rich oligomer under study existed in a stable parallel G-quadruplex form even at a denaturing temperature of 95°C (Figure S1F), explaining the observed multiple bands (intra- and intermolecular G-quadruplex forms) even on a denaturing PAGE (Figures 1B and S1C). Thus, our results suggest that oligomeric DNA substrates capable of forming G4 structures *in vitro* exhibit resistance to IR-induced DNA cleavage.

G4-forming Human Genomic Regions when Present as Short DNA Fragments Are Protected from IR-induced DNA Breaks

Based on the above results, we were interested in investigating whether regions from the human genome known to form G4 structures, when present on a shorter oligomeric DNA, can exhibit a shielding effect against radiation. To test this, three independent human genomic regions, *VEGF* promoter, *HIF1α* promoter, and the telomeric repeats, known to form stable G4 structures were selected and the formation of the structure was confirmed by EMSA and CD analyses (Agrawal et al., 2013; Nambiar et al., 2011; Sun et al., 2011) (Figures S1H–S1J). DNA oligomers were allowed to fold into G-quadruplex and investigated for their radiation sensitivity, as compared with either complementary sequence or random sequence with same length and GC content (Figures 1J, S1H, and S1I). Interestingly, the G4 oligomers showed reduced cleavage intensity, in comparison with their respective complementary or random sequence, in the case of all three regions (Figures 1J, 1K, S1H, and S1I). Further, when double-stranded oligomeric DNA spanning three different regions from telomeric DNA were subjected to increasing doses

of IR, a dose-dependent increase in radiosensitivity was observed (Figures 1L–1N). Thus, as a proof of principle, we found that three independent regions from the human genome that can fold into G-quadruplex structures exhibited reduced IR-sensitivity, as compared with the respective control DNA sequences. Although we observed background cleavage at G-rich oligomers even in absence of radiation, the result obtained was significant, because the substrate provided in either of the cases was not limiting, and the irradiation did not lead to an over and above increase in cleavage, unlike C-rich strand.

The Planar Quartet in a G4 Structure Is Resistant to IR-induced DNA Damage

Having studied the *in vitro* shielding effect of a G-quadruplex structure against IR, we were interested in exploring the mechanistic details of the phenomenon. A typical G4 structure is formed by Hoogsteen hydrogen bonding between the N7 position of guanine residues, resulting in a planar quartet composed of four such guanines (Mirkin, 2013; Nambiar et al., 2011; Sinden, 1994).These quartets are stacked upon each other and connected by a single-stranded intervening loop sequence comprising of the same strand (intramolecular G4) (Figure 2A) or different strands (intermolecular G4) (Bochman et al., 2012; Nambiar et al., 2011). In order to investigate the differential sensitivity between the planar quartet and the single-stranded loop region, we resorted to the DMS protection assay. Quadruplex-forming oligomers derived from G-rich sequence of *BU1A* gene (Schiavone et al., 2014) or a random DNA were irradiated, treated with dimethyl sulfate (DMS), and resolved on an 18% denaturing PAGE (Figures 2A and 2B). Interestingly, a distinct increase in the cleavage intensity at intervening loop sequences was observed upon irradiation (Figure 2B, lane 2). However, there was no significant change in the intensity of bands due to DMS chemical probing at the guanine residues involved in G4 formation (Figure 2B). In order to investigate the radiosensitivity of a guanine residue, which is not involved in structure formation, a random sequence containing stretch of guanines was examined following DMS protection assay. Results showed enhanced cleavage at the two individual guanines, as compared with those involved in intermolecular G4 formation (Figure 2B, lanes 3,4). Further, when an oligomeric DNA harboring either the human telomere repeat sequence (established to form a G4 structure *in vitro*) or the known G4 structure-forming sequences from *BCL2* and *HOX11* regions were employed, a consistent cleavage preference toward the intervening loop sequence was observed (Figures 2C and 2D), unlike the guanine stretches. Interestingly, a loop length of 2 nt was sufficient to result in IR-induced DNA break (Figures 2B and 2D). Thus, our results suggest that the planar quartet formed in a G4 structure is resistant to IR-induced DNA strand-breaks, as opposed to the single-stranded loop region.

Formation of G-Quadruplex Structures Provides Shielding Effect against γ-Radiation-induced DNA Breaks

Previous studies have reported lower oxidation potential of G4 planar quartet, as compared with individual guanine residues (Choi et al., 2013; Lech et al., 2013; Wu et al., 2015). Based on our observations, and the information available in literature, we postulate a mechanistic model for shielding effect of a G-quadruplex structure against radiation-induced DNA damage (Figure 2E). IR induces radiolysis of water, leading to generation of highly reactive free radicals within the cell. Hydroxyl radicals cause breakage of the sugar-phosphate backbone by abstracting an H atom from the deoxyribose sugar unit in the DNA (Balasubramanian et al., 1998; Breen and Murphy, 1995). G4 structures exhibit reduced IR-induced DNA damage, possibly owing to the lower oxidation potential of the planar quartet, than individual guanines, and its free radical trapping property, which needs to be explored further (Figure 2E).

Evaluation of IR-induced DNA Breaks on Other Non-B-DNA Forms

Based on the observed radioprotection seen in G4 DNA, we were interested in studying the effects of irradiation-induced damage on other non-B-DNA structures such as hairpin and triplex DNA (Figures 2F and S2). Results showed that unlike G4-forming regions, five different hairpin-forming oligomers (Hp1–Hp5) were sensitive to IR (100 Gy) (Figures 2G–2I). Preliminary studies suggest that when triplex DNA was subjected to increasing doses of radiation (0, 10, 20, 50, 100, 200 Gy), there was no detectable increase in the DNA cleavage unlike duplex DNA control (Figure S2). Formation of triplex DNA was confirmed by native PAGE following incubation of radiolabeled duplex DNA with a third strand in appropriate incubation buffer (Figure S2B). The mechanism for resistance of triplex toward radiation-induced damage needs to be investigated further.

Therefore, our results reveal that different forms of DNA may provide differential sensitivity to radiation. Although a sequence-independent cleavage was observed when single-stranded DNA, double-stranded DNA, and hairpin DNA were irradiated, formation of G4 DNA and triplex DNA showed reduced or no sensitivity to radiation (Figure 2J).

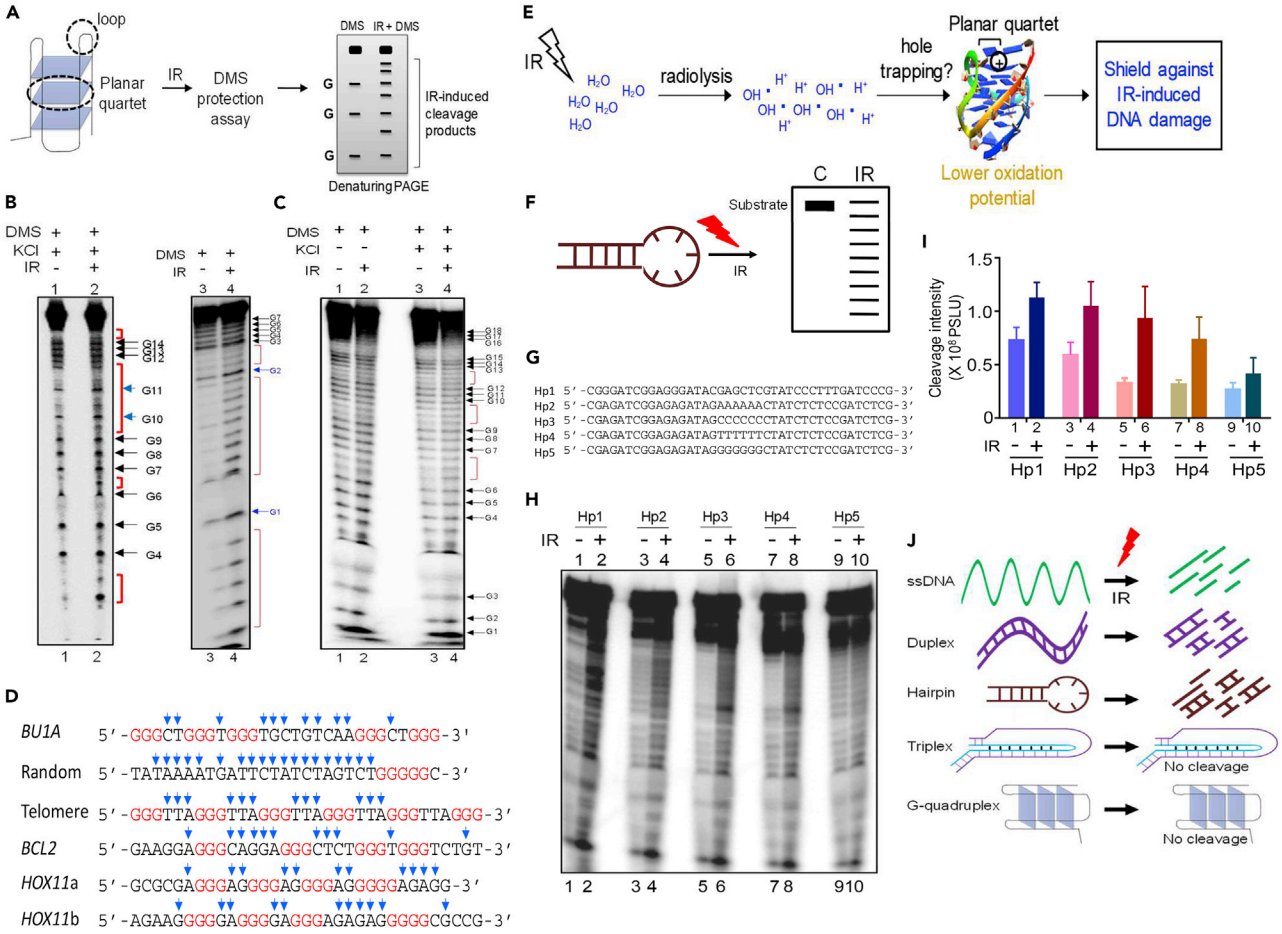

Figure 2. Evaluation of Radiation Sensitivity of Different Forms of DNA Structure when Present on an Oligomeric DNA

(A) Strategy for evaluating radiosensitivity of planar quartet region in a G4 structure, as opposed to single-stranded loop region using DMS protection assay.

(B and C) Effect of radiosensitivity of guanine residues when present in the loop region as compared with a Hoogsteen hydrogen-bonded region when a G4 DNA derived from *BU1A* gene was used. The G4 motif and a random DNA (B) were evaluated for radiosensitivity of the loop region following DMS chemical probing. Guanine residues not involved in planar quartet formation are indicated by blue arrow. Assessment of telomere oligomers for differential sensitivity of the planar quartet (GGG) as compared with the intervening loop sequence (TTA) is also shown (C). Individual guanine position is marked by black arrows, whereas red brackets denote loop in both the panels. 100 mM KCl was used for stabilization of the G4 structures.

(D) Comparison of IR sensitivity at loop regions of various G4 DNA motifs derived from different genes (*BU1A*, Telomere, *BCL2*, *HOX11a*, and *HOX11b*). Sequences of DNA substrates used are shown. Guanines are indicated in red, whereas loop regions are in black. Radiation sensitive nucleotides are indicated using blue arrow. An oligomer containing random DNA sequence is also used for the study.

(E) Proposed model for shielding effects against radiation-induced damage by G4 planar quartets. Radiation affects water molecules in a cell (radiolysis) to form reactive oxygen species, which in turn causes single- and double-strand DNA breaks in the genome. However, the planar G4-quartet acts as a shield against radiation-induced DNA damage owing to potential reasons such as lower oxidation potential and hole trapping properties of the G4 quartet, thus imparting the property of radioresistance.

(F–I) Evaluation of radiosensitivity on DNA sequences that can fold into different hairpin structures. Schematic representation of evaluation of IR-induced DNA strand-breaks on hairpin DNA substrates, Hp1–Hp5 (F and G). PAGE profile showing radiosensitivity on different hairpin DNA structures. Following γ-irradiation (100 Gy), hairpin-forming oligomers were resolved on a denaturing PAGE, along with their respective unirradiated controls and analyzed for the abundance of DNA breaks (H). In each case, the intensity of IR-induced cleavage and its respective unirradiated control was quantified (n = 3) and plotted (I). Bar graph shows mean ± SEM.

(J) Schematic showing summary of observed sensitivity of different forms of DNA at the IR doses investigated.

See also Figure S2.

Radiation Causes Minimal Damage at the Telomeres Inside Cells

The observation that telomere repeats when folded into a G-quadruplex structure can protect from radiation encouraged us to investigate whether telomeres on a human chromosome are sensitive to radiation inside cells, as it is well established that telomeric DNA can fold into G-quadruplex structures inside the

cells. K562, MCF7, and HeLa cells were irradiated, allowed to recover partially, and assessed for DDR signals at the telomeres using immunofluorescence (green signal) and FISH (red signal) marking either 53BP1 or γH2AX and telomere repeats, respectively. The readout of the assay was based on the degree of colocalization between the two signals, post-irradiation, suggesting either intact telomere (no colocalization) or those harboring DNA strand-breaks (colocalization of signals) (Figure 3A). Each cell was analyzed for the extent of colocalization, independently in case of green over red and red over green signals, using ImageJ software and presented as independent IR (green colored) and IR (red colored) box-and-whisker plots.

Interestingly, we did not find significant colocalization between telomeric FISH signals and γH2AX or 53BP1 foci, when examined in K562 and MCF7 cells following irradiation, suggesting intact telomeres post-IR treatment (Figures 3B–3E, S3A, and S3B). As expected, sham control cells did not show much 53BP1/γH2AX staining, confirming IR-specific foci generation in the experimental samples (Figures 3B, S3A, and S3B). Furthermore, no colocalization of 53BP1 and FISH signals was detected post-irradiation, when an independent cell line, HeLa, was used for the study (Figures 3F and 3G). Colocalization analyses between 53BP1 foci and centromeric FISH signals following irradiation revealed significant colocalization coefficients, suggesting colocalization of both the signals elsewhere, unlike that observed in the case of telomeres (Figures 3H and 3I). Colocalization between γH2AX and 53BP1 served as positive control (Figures 3J and 3K).

We performed a co-immunofluorescence for TRF2, one of the members of shelterin complex (Lazzerini-Denchi and Sfeir, 2016) with γH2AX, following exposure to IR with a 30 min recovery period and found no colocalization between the two signals (Figure 3L). Taken together, our data suggest that radiation was unable to induce DSBs at the telomeric ends. Further, to investigate whether knockdown of TRF2 can lead to disassembly of shelterin complex allowing recruitment of 53BP1 to telomere ends, we performed IF-FISH following TRF2 knockdown in HeLa cells (Figure S3C). Results showed significant colocalization of telomere probes and 53BP1 (Figures S3D and S3E) as reported before (Lackner et al., 2011; Mao et al., 2007). Thus, these results show that there is no colocalization of DSBs with telomere, upon irradiation, when multiple cell lines were used.

Genome-wide Presence of G4 Motifs Explains Variation in Radiation Sensitivity among Chromosomes

In order to investigate variation in IR-sensitivity across the genome, we analyzed human genomic data derived from control and irradiated (5 Gy) samples. Data were downloaded from the online SRA study (Project ID: ERP004219), mapped, and aligned against the hg38 reference genome and viewed in the Integrated Genome Viewer (IGV). DNA breaks induced following exposure to radiation interrupt the continuity of the genome, leading to loss of reads on such templates. Interestingly, results showed that multiple locations across the genome exhibited stretches of at least 1000 base pairs with no reads (0 coverage), whereas corresponding locations in unirradiated controls showed acceptable coverage ($\geq$5 reads) (Figure 4A). The regions with zero reads are termed as "damaged sites" (stretches of broken DNA) in further study.

Having defined the broken regions in the human genome upon irradiation, percentage of damaged sites across chromosomes and the number of G4 motifs in the damaged regions (using the online Quadparser database) (Wong et al., 2010) were assessed (Figure 4B). Results showed that although overall GC content of chromosomes was comparable (~42%), chromosome 9, 13–16, 21, and 22 were more sensitive to radiation (Figure 4B). Importantly, these chromosomes harbored less number of G-quadruplex-forming motifs.

The retrieved data was further analyzed using hclust. Results showed two defined clusters of the chromosomes, with a median of 15% (Figures 4B and 4C). Interestingly, among the unprotected regions, chromosomes with higher DNA damage (>15%) harbored less number of G4-forming motifs (8–25/mb), whereas chromosomes with <15% damage harbored higher number of G4 motifs (35–72/mb) (Figure 4C). The regions of higher damage were 6–15 kb in length unlike those with lesser damage (1–2 kb) and harbored less G4 motifs. This suggested a significant inverse correlation between the number of G4-forming motifs, and extent of damage within the genome, upon irradiation (Figure 4C). The above data were statistically significant, as assessed and confirmed using multiple statistical tests such as Student's t-test ($p = 0.0001$), Mann-Whitney U test ($p = 0.0001$), and Pearson correlation coefficient (R value of −0.82). Although the GC content of each chromosome was observed to be in the same range, noteworthy variations in IR

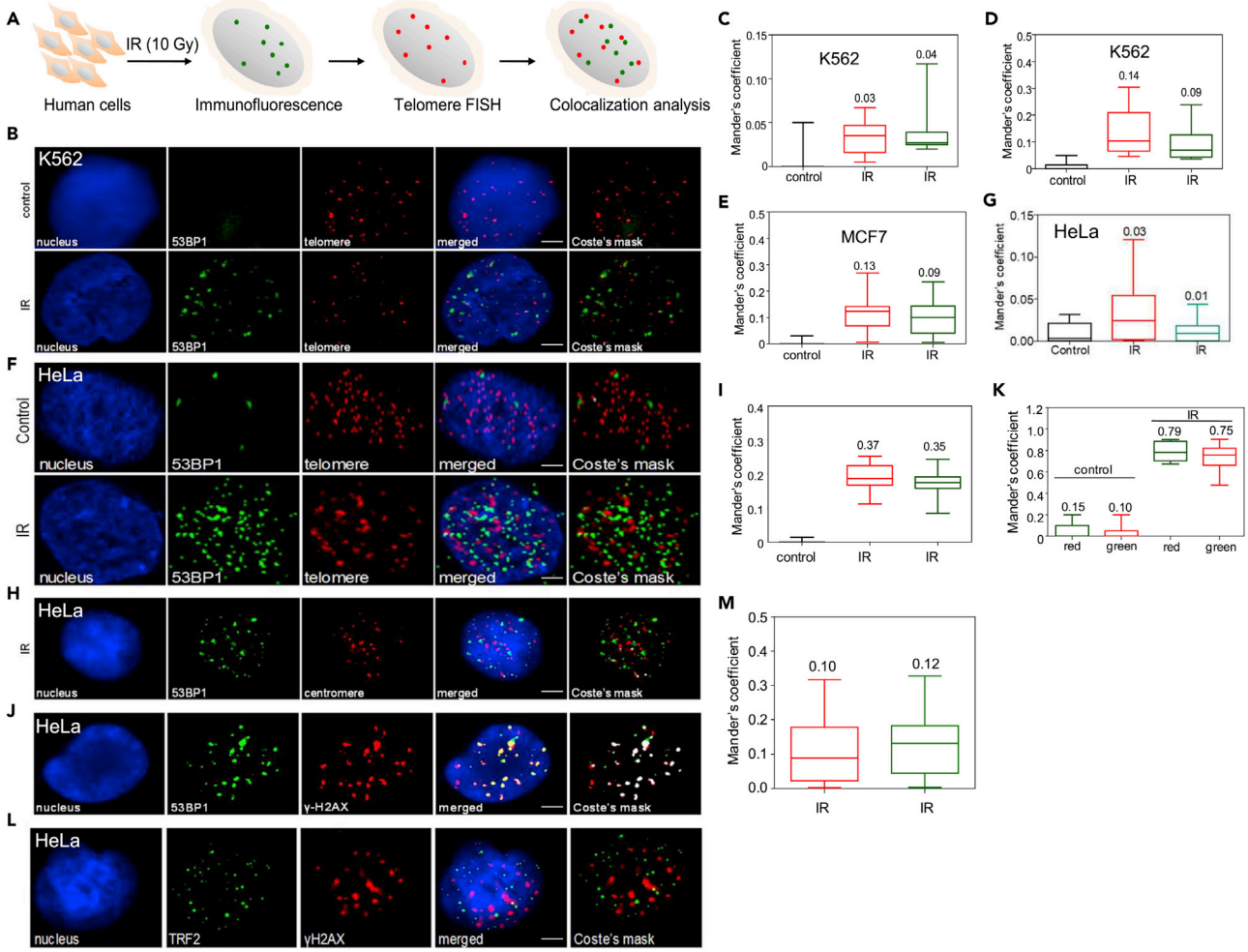

Figure 3. Evaluation of Induction of DNA Double-Strand Breaks at Human Telomeric Region within the Cells Following Exposure to IR

(A) Strategy used for assessing IR-induced DNA breaks at telomeres inside cells. Cells were exposed to IR (10 Gy), incubated for 30 min to allow DNA damage marker proteins (53BP1 and γH2AX) to form distinct foci. Post-IF, cells were subjected to telomere FISH to mark the telomeres within cells, followed by colocalization analysis of the two signals.

(B) Representative IF-FISH images of K562 cells following irradiation with IR. K562 cells were irradiated, followed by IF to detect 53BP1 foci (green; FITC), FISH to demarcate telomeres (red; TTAGGG-Cy3), and DAPI staining for nucleus (blue). Multiple "Z stacks" were captured in case of every image, and the resulting images were stacked to give the "merged" image.

(C–E) Box-and-whisker plots depicting Mander's colocalization coefficient (range 0–1; "0" signifying no colocalization and "1" signifying 100% colocalization) as evaluated by JACoP plug-in of ImageJ software. Experiments were performed in two independent cell lines, K562 (C, D) and MCF7 (E) as described above, quantified, and presented. Although 53BP1 was used to detect DNA breaks in panel C, γH2AX was used for panels D and E. A minimum of 100 cells were analyzed for colocalization of red and green signals and plotted as the fraction of red overlapping green (box-and-whisker plot shown in red) and green overlapping red (box-and-whisker plot shown in green). The observed median value is indicated above the respective graph. Control refers to colocalization analysis performed in non-irradiated samples.

(F) Representative IF-FISH images following irradiation in HeLa cells. Irradiated cells were subjected to IF using anti-53BP1 (green; Alexa Fluor 488), FISH to demarcate telomeres (red; TTAGGG-Cy3), and DAPI staining for nucleus (blue). Multiple "Z stacks" were captured and the resulting images were stacked to give the "merged" image as above.

(G) Box-and-whisker plots depicting Mander's colocalization coefficient (range 0–1; "0" signifying no colocalization and "1" signifying 100% colocalization) as evaluated by JACoP plug-in of ImageJ software. Experiment was performed in HeLa cells as described above, quantified, and presented.

(H) Representative IF-FISH images showing localization of 53BP1 foci (green) and centromere (red). A Coste's mask, depicting merge of green and red foci (merged foci shown as white dots depict true colocalization), is also shown in the extreme right panel.

(I) Box-and-whisker plot depicting Mander's colocalization coefficient for green (53BP1) and red (centromere) signals. The median values have been indicated above respective graphs. Each experiment was analyzed by evaluating a minimum of 100 cells.

(J) Representative IF images showing colocalization of 53BP1 and γH2AX in HeLa cells following irradiation (10 Gy). 53BP1 is depicted in green (FITC), γH2AX in red (Alexa Fluor 568), and nucleus in blue (DAPI). Merged image, showing colocalized yellow foci is presented, along with Coste's masked image with white dots indicating true colocalization.

Figure 3. *Continued*

(K) Box-and-whisker plot showing Mander's colocalization coefficient (range: 0–1) for experiments shown in panel J.

(L) Co-IF for TRF2 and γH2AX in HeLa cells. Cells were irradiated (5 Gy), allowed to recover (30 min), and immunostained for TRF2 (FITC; green) and γH2AX (Alexa Fluor 568; red). Nucleus was counterstained using DAPI (blue), and a merged image consisting of all three channels is shown. Images were subjected to colocalization analysis as above and a Coste's mask depicting colocalization between red and green signals was generated.

(M) Box-and-whisker plot showing Mander's colocalization coefficient for experiments shown in panel L.

In panels B, F, H, J, and L, scale bar indicates 2 μm.

See also Figure S3.

sensitivity among chromosomes suggest that G4 structures are responsible for the observed differential sensitivity to radiation.

Further, to investigate the distribution of G4 motifs and IR sensitivity in promoter regions, the sequences from unprotected regions were segregated and fragments mapping to the promoters were determined. Interestingly, only 6% of the unprotected fragments mapped to promoters, whereas the rest were at the protected region (Figure 4D). Importantly, 98.3% of the G4-forming motifs were present at the protected regions. When coding regions were analyzed in a similar manner, 4% of the unprotected fragments mapped to the CDS, which harbored only 11% of G4 motifs (Figure 4D). In contrast, 89% G4 motifs were present in the protected CDS (Figure 4D).

Similar study was extended to an irradiated human sample (10 Gy), which was downloaded from the SRA study (Project ID: SRP022845). Irradiated DNA sample was analyzed as described above using same parameters. Results showed that the regions of chromosomes with more DNA damages (>7%) harbored less number of G4-forming motifs (3–47/mb) per damaged region, whereas chromosomes with less damaged region (<7%) harbored more number of G4 motifs (92–320/mb), suggesting an inverse correlation as observed above (Figures S4A and S4B). Statistical evaluation using Student's t-test and Mann-Whitney U-test (p value<0.0001) further confirmed the level of significance. An inverse correlation was confirmed using Pearson correlation analysis (R value −0.80). High-throughput sequence analyses of unprotected regions, which were classified as promoters, and CDS based on their mapping to respective regions on the chromosome revealed ~22% of the unprotected fragments both from promoters and CDS with 11 and 0.4% G4 motifs, respectively (Figure S4C). In contrast, 89 and 99.6% G4 motifs were present in protected regions of promoters and CDS, respectively (Figure S4C). Thus, results suggest that irrespective of the dose used (5 or 10 Gy), presence of G-quadruplexes contributes to reduced radiosensitivity in the genome.

G4-Forming Regions in Cells Remain Intact upon Radiation Exposure

To experimentally confirm the above findings, twelve regions known to form G4 structures and matching control regions (that did not harbor G4 forming motifs) were amplified from genomic DNA isolated from human cells (Nalm6), post-irradiation. Because DNA breaks generated following irradiation can result in reduction in the number of template strands available for amplification, efficiency of PCR will be less compared with an unirradiated control. Thus, the difference in amplification between control (−IR) and irradiated (+IR) genomic DNA can serve as a measure to assess the intactness of the particular genomic DNA region (Figures 5A and S5A). Genomic DNA was irradiated with an increasing doses of IR (1, 1.5, and 2 kGy), and formation of subsequent DNA strand-breaks was confirmed on an agarose gel (Figure S5B). In order to score for the reduced template due to breakage of DNA strands in genomic regions using PCR, we employed a high radiation dose. Interestingly, random regions showed a dose-dependent decrease in amplification, as compared with that of the controls, suggesting IR-induced DNA breaks at the template sequence (Figures 5B, 5C, and S5C). Surprisingly, in case of regions containing G4-forming motifs, nine out of ten regions showed no significant difference upon amplification, suggesting the presence of intact sequence post-irradiation (Figures 5B and 5C). Interestingly, it has been shown that sequences with alterations in the canonical formula (for example, those involving larger loop lengths, DNA bulges, two-plate sequence, GNG motifs etc.) can also fold into G-quadruplex forms (Chambers et al., 2015; Das et al., 2016). Although most of the regions under study possessed canonical G-quadruplex-forming sequences, four regions were capable of forming G4-DNA structures (as analyzed by multiple softwares including Quadbase and QGRS mapper) (Kikin et al., 2006; Yadav et al., 2008) inspite of harboring noncanonical G-quadruplex sequences. *KRAS*, which exhibited reduction in PCR amplification efficiency even though a G4 motif was present, warrants further investigation (Figures 5B and 5C).

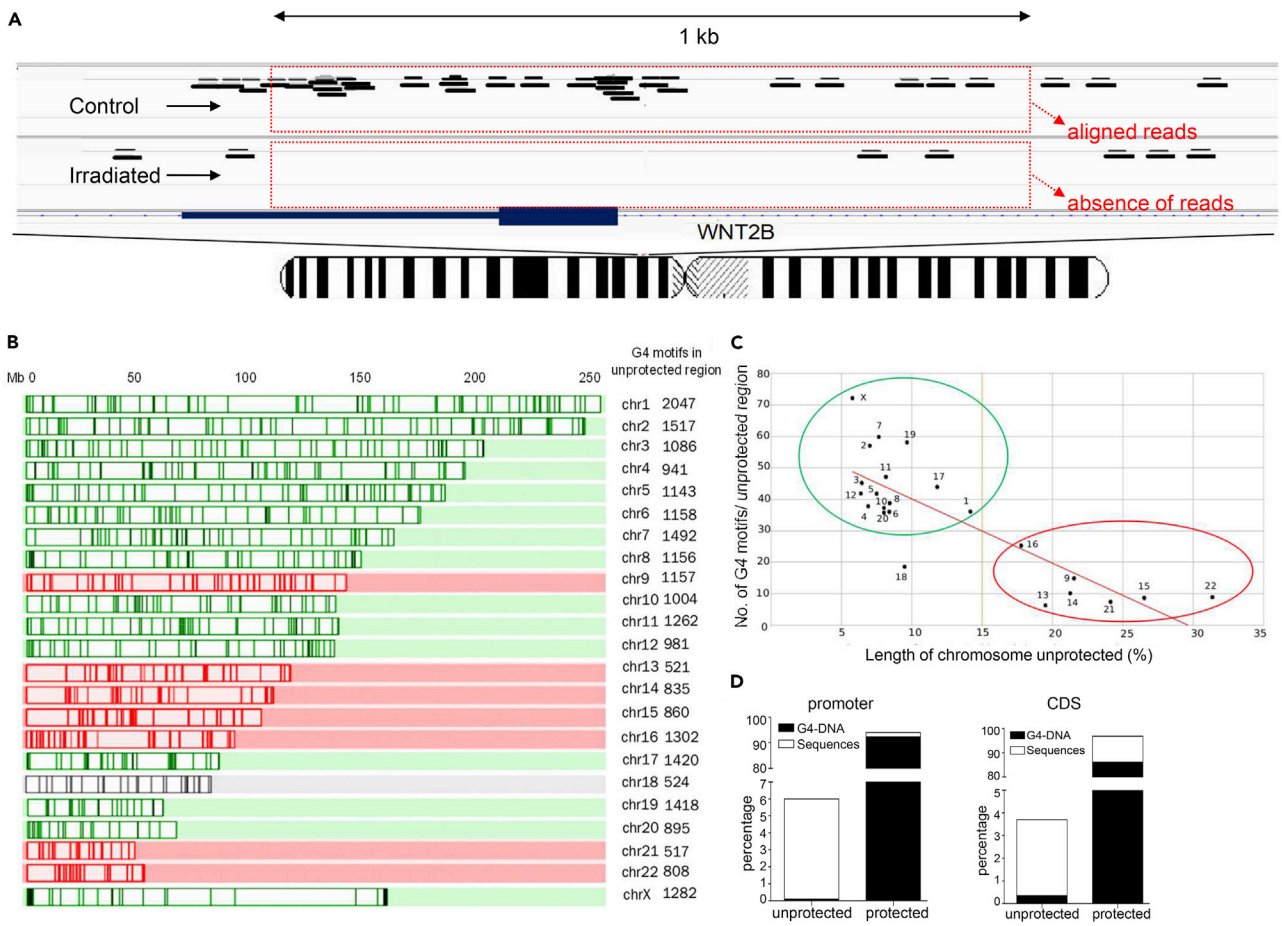

Figure 4. Evaluation of Human Genome Sequences for Their Sensitivity toward IR

(A) DNA sequences from human genome were evaluated to determine the unprotected regions and the frequency of occurrence of G-quadruplex region in it compared with protected sequences. A minimum length of 1000 bp or greater was analyzed from whole genome. The human genome sequenced files deposited in SRA (Sequence Read Archive) database; sra-id: ERP004219 from control and irradiated human cells (5 Gy) have been downloaded and used for the study. The control input DNA sequence shows aligned reads, whereas the irradiated sample did not have reads in several locations.

(B) A representative set of 1% of unprotected regions in every chromosome. Chromosomes with higher amount of breakage are colored in red and the ones with less breakage are in green. Every bar represents a chromosome with the corresponding length to the scale and each line on the bar represents the location of the unprotected region.

(C) A scatterplot showing inverse correlation between percentage of unprotected length in each chromosome versus the number of G4 motifs per unprotected region.

(D) Stacked bar graphs showing genome-wide analysis of number of G4 motifs harbored by protected and unprotected regions of irradiated CAL51 cells, in the promoter (left panel) and coding DNA sequence (right panel). In both the cases, the white bar represents the percentage of total sequence analyzed, whereas the black bar represents percentage of G4 motifs.

See also Figure S4.

To verify the above findings, the amplification was performed using real-time PCR and changes in Ct values obtained for control and irradiated samples were analyzed. Interestingly, the G4-forming motif present in *VEGF* did not show a significant change in the Ct value upon irradiation, whereas an identical sized region devoid of a G4-forming motif, taken from the same gene, showed an IR-dose-dependent increase in the Ct value (Figure 5D, upper panel). Results were reproducible in an independent region of *MYC* promoter (harboring G4 motif), when compared with a random region from the same gene (Figure 5D, lower panel). Analyses of 22 independent genomic regions showed significant differences between amplification in control and IR-treated samples (Figure 5E). The set of ten random regions showed a significant increase in Ct values when irradiated samples were used, whereas it was minimal for G4-forming regions (Figure 5F). Taken together, real-time analyses of irradiated DNA samples demonstrated noteworthy protection by G4-forming regions, as compared with the rest of the genome. It is known that G4 structures stall polymerases *in vitro* and

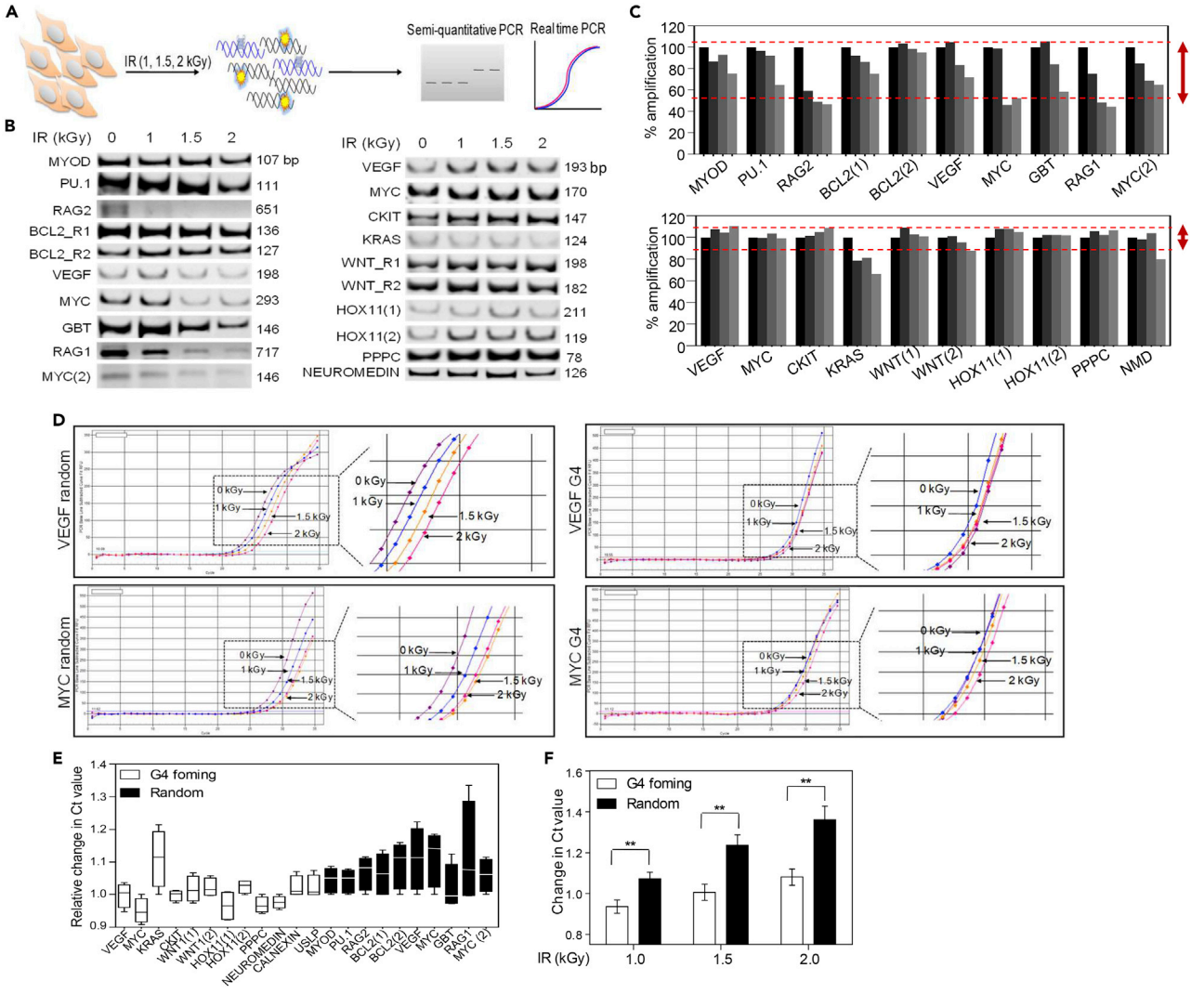

Figure 5. Real Time Analyses of Impact of Various G4 Motifs on DSB Generation in the Human Genome Following Irradiation

(A) Experimental strategy to assess intactness of independent G4-forming motifs inside the cells in comparison with size-matched random sequences, which do not support formation of G4 structures. Cells were irradiated with increasing dose of γ-radiation (1, 1.5 and 2 kGy), genomic DNA was extracted immediately and used for PCR amplification of region of interest. Each set of G4-forming regions and random ones was evaluated by genomic polymerase chain reaction (PCR) and real-time PCR.

(B) Gel profile showing genomic PCR products for control and irradiated samples (1, 1.5, and 2 kGy) for G4-forming regions, *VEGF, MYC, CKIT, KRAS, WNT*(1), *WNT*(2), *HOX11*(1), *HOX11*(2), *PPPC*, and *NEUROMEDIN* (right panel), and regions devoid of G4 motifs, *MYOD, PU.1, RAG2, BCL2*(1), *BCL2*(2), *VEGF, MYC, GBT, RAG1*, and *MYC*(2) (left panel). The size of each region amplified has also been indicated.

(C) Bar graphs depicting percentage amplification in various regions forming G4 structures (lower panel), as compared with the region devoid of a G4 motif (upper panel). For each region, the amplification of irradiated samples is normalized with respect to that in the control sample (considering it as 100%). Red dotted lines demarcate highest and lowest amplification values on an average for both the datasets, denoting the difference in amplification in each sample.

(D) Representative real-time PCR profiles of G4-forming region of *VEGF* (upper right panel), its random counterpart (upper left panel), G4-forming *MYC* (lower right), and its random sequence (lower left) are presented. Individual amplification profiles for each dose have been enlarged, boxed, and indicated with arrow and shown on the right in all 4 profiles.

(E) Box-and-whisker plot showing relative change in Ct value in case of twelve G4-forming motifs (white boxes) and ten random regions (black boxes), as determined by real-time PCR. The height of the bar indicates difference in amplification in control, as compared with that in irradiated samples, indicating a measure of intactness of the respective region.

(F) Bar graph showing change in Ct value across all twenty-two regions tested, normalized with respective unirradiated control value. In each case, G4-forming regions (white bars) and random regions (black bars) are plotted for three independent radiation doses with error bars showing mean ± SEM (ns: not significant, *$p < 0.05$, **$p < 0.005$, ***$p < 0.0001$).

See also Figure S5.

in vivo, and hence could lead to a decreased amplification of those regions upon PCR. However, in our analyses, amplification in each irradiated genomic region was compared with its respective unirradiated control to gauge the intactness of that region and thus, this caveat did not bias the observation.

Formation of G4 DNA Contributes to Genome-wide Radioprotection and Can Be Modulated by G4 Resolvase Inside Cells

To evaluate formation of G4 structures in a genome-wide manner, we resorted to the use of a previously characterized G-quadruplex-specific antibody, BG4, which binds to G4 structures inside cells (Biffi et al., 2013, 2014). Following irradiation (10 Gy), HeLa and MCF7 cells were subjected to IF using purified anti-BG4 (Figures S5D and S5E) and anti-γH2AX and analyzed for colocalization signals (Figures 6A and 6B). Results showed no significant colocalization between the damage-induced foci and the BG4-bound quadruplex regions, suggesting that G4 structures inside cells were unaffected, post-IR (Figures 6A–6D). Interestingly, use of low and high doses of irradiation (5, 20 Gy) did not show any significant colocalization between γH2AX foci and the BG4 foci (Figures 6E and 6F). Further, to test whether stabilization of G4 structures inside cells would impart additional protection against IR-induced DNA damage, we used a known G4 stabilizer, TMPyP4, to stabilize quadruplexes in HeLa and MCF7 cells, followed by exposure to radiation (10 Gy) and assessment of DNA damage by 53BP1 staining (Figures 6G and S6A). Results showed a significant increase in the number of cells devoid of 53BP1 foci, along with a concomitant decrease in cells harboring multiple foci, upon TMPyP4 treatment, as compared with irradiation alone (Figures 6G–6I and S6A). Although DNA damage induction by TMPyP4 is reported previously (Cheng and Cao, 2017), in order to investigate the radiosensitivity upon G-quadruplex stabilization, we employed a lower dose of the stabilizing agent that did not induce any damage by itself (data not shown). Further, we investigated the effect of an independent G-quadruplex stabilizing agent, pyridostatin, on radiation-induced DNA DSBs in cells by employing both immunofluorescence and comet assays. Although pyridostatin by itself has been shown to induce DNA damage (Rodriguez et al., 2012), (data not shown), use of a lower concentration (2 μM) did not result in any DSB induction on its own. 53BP1 staining after pyridostatin treatment showed significant decrease in DNA damage-induced foci in MCF7 cells owing to G-quadruplex stabilization; however, the impact was limited in HeLa cells (Figures 6J, 6K, and S6B). Comet assay results revealed decreased DSB-induction in pyridostatin-treated cells, after radiation, as compared with irradiation alone controls in HeLa cells (Figures S6C and S6D).

Werner (WRN) is one of the RecQ family helicases, known to resolve G-quadruplex structures in the genome (Chu and Hickson, 2009; Mendoza et al., 2016). We investigated the impact of modulation of WRN expression on radiosensitivity in HeLa cells. Interestingly, we observed significant decrease in radiation-induced DSBs upon knockdown of WRN helicase, as compared with scrambled control transfection (Figure 7). In contrast, overexpression of WRN resulted in significant increase in the number of 53BP1 foci (Figures 7B–7D). Further, DSB formation by IR was also investigated after WRN knockdown followed by its overexpression (Figure 7B). Results showed significantly improved number of 53BP1 foci upon irradiation in these cases (Figures 7C and 7D). Similar results were also observed when Nalm6 cells were irradiated following knockdown or overexpression of WRN using comet assay or 53BP1 foci formation assay (Figure S7).

Taken together, our findings reveal that stabilization or modulation of G-quadruplex resolving helicases inside cells has a direct impact on radiosensitivity, thus further establishing the role of G-quadruplex structures in shielding the genome against radiation.

DISCUSSION

Our findings establish that the human genome is not uniformly susceptible to ionization radiation and hence DNA strand-breaks. Sequences of the genomic region play a significant role toward its sensitivity to IR. Specifically, our data demonstrate that G-quadruplex structures when formed at GC-rich stretches of genome could reduce sensitivity to radiation-induced DNA damage, as compared with their B-DNA counterparts within cells.

Conformation of the DNA, but Not the Sequence, Governs Sensitivity to Radiation

IR affects DNA in a multitude of ways such as base or sugar damage, single- and DSB formation, DNA interstrand cross-linking, and DNA-protein cross-linking (Lomax et al., 2013). Oxidative damage to the DNA

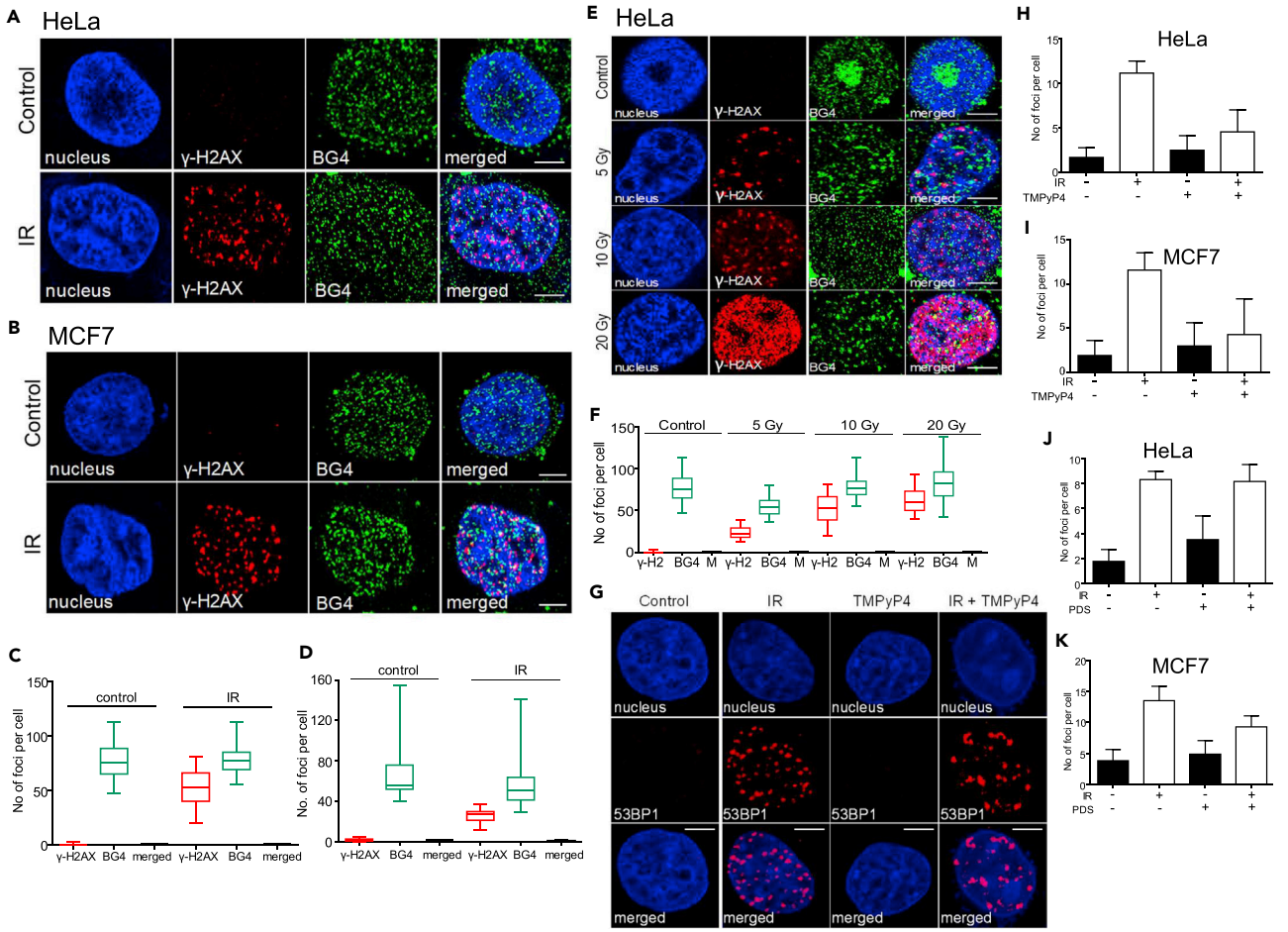

Figure 6. Assessment of Genome-Wide Radio-Protection Contributed by G4 Structures Inside Cells

(A and B) Representative immunofluorescence images to determine colocalization of G-quadruplex structures and IR-induced DNA breaks. Irradiated HeLa (A) and MCF7 (B) cells (10 Gy) were incubated for 30 min to allow DNA damage response to initiate and evaluated by IF using anti-BG4 antibody (Alexa Fluor 488; green) and anti-γH2AX antibody (Alexa Fluor 568, red). Nucleus is stained with DAPI (blue). The channels were merged and subjected to colocalization analysis using JACoP plug-in of ImageJ software.

(C and D) Box-and-whisker plot showing quantification of the number of BG4 or γH2AX foci per cell in HeLa (C) and MCF7 (D) cells. Number of cells that show merge of both antibodies are also shown. In each case, a minimum of 100 cells were counted and the resulting population analyses has been shown.

(E) Representative immunofluorescence images showing colocalization of G-quadruplex structures (detected using BG4) and DNA breaks (detected using γH2AX). Irradiated HeLa cells (5, 10, and 20 Gy) were evaluated as described above.

(F) Box-and-whisker plot showing quantification of the number of foci per cell (γH2AX alone, BG4 alone, and merged) following exposure to increasing dose of IR (5, 10 and 20 Gy) in each case, a minimum of 50 cells were counted and presented. "γH2" represents γH2AX.

(G) Evaluation of impact of G4 DNA stabilizers on radiation-induced DNA strand-breaks within HeLa and MCF7 cells. Representative images showing effect of TMPyP4 on radiation-induced breaks in HeLa cells (G). Cells were treated with TMPyP4 (5 μM, for 5 hr), irradiated (10 Gy; 30 min recovery period), and immunofluorescence was performed using anti-53BP1. The images show 53BP1 binding as red foci (Alexa Fluor 594) and nucleus as blue (DAPI). Merged images comprising of both the channels are shown in the lower panel.

(H and I) Bar graphs showing quantification of 53BP1 foci per cell following irradiation in cells treated with TMPyP4 in HeLa (H) and MCF7 (I), as described above.

(J and K) Bar graphs showing quantification of 53BP1 foci per cell following irradiation (10 Gy; 30 min recovery period) after treatment with G4 stabilizer pyridostatin (PDS, 2 μM; 5 h) in HeLa (J) and MCF7 (K).

In panels A, B, E, and G, scale bar indicates 5 μm. In panels H–K, a minimum of 200 cells were counted and in each case bar graph shows mean ± SEM. See also Figures S5C, S5D, and S6.

results in formation of various products such as 8-oxo-guanine; 8-oxo-adenine; 5,6-thymine glycol; 2-hydroxyadenine; and FapyA and FapyG lesions (Cooke et al., 2003). Among the four DNA bases, Guanine is the most sensitive to oxidative damage by IR, 8-oxo-G being the most common and stable oxidation product (Kasai and Nishimura, 1984; Ohno et al., 2006). In line with this, previous studies have reported

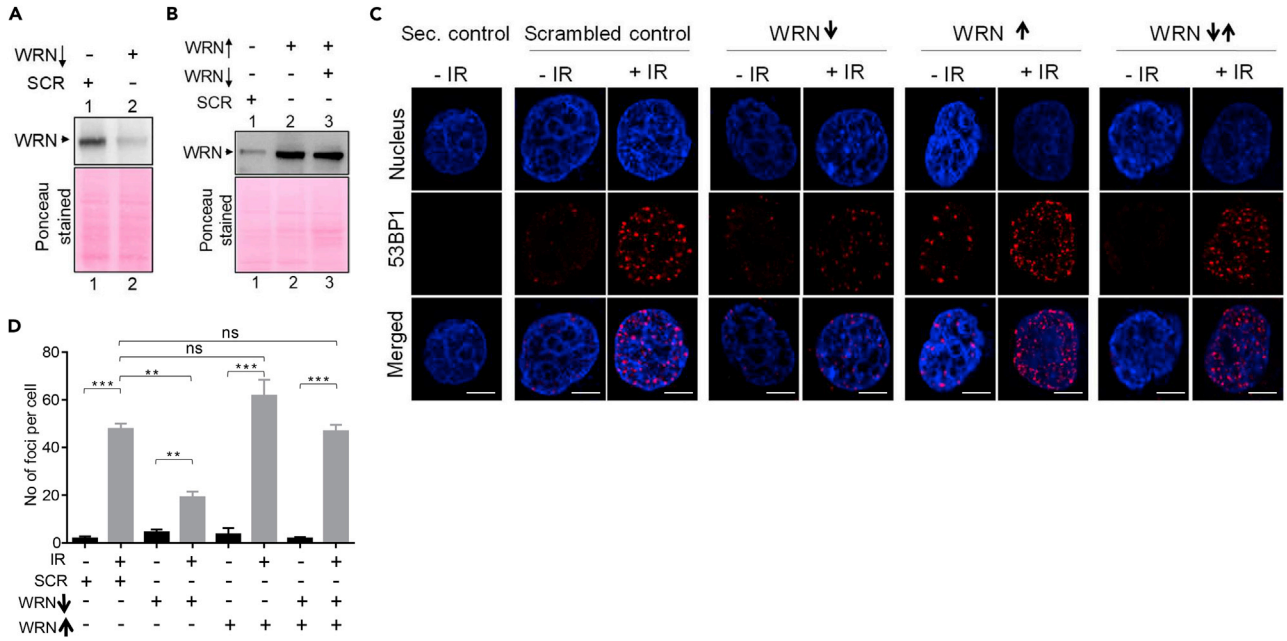

Figure 7. Modulation of Radiosensitivity of Genome Following Downregulation or Upregulation of WRN Helicase Inside Cells

(A and B) Representative Western blot showing level of WRN helicase in HeLa cells following either its knockdown by transfecting shRNA plasmids, upon WRN overexpression or after WRN overexpression following its knockdown. A plasmid with scrambled sequence was used as control during transfection. Ponceau-stained blot served as a loading control.

(C) Representative immunofluorescence images showing 53BP1 foci formation (red, Alexa Fluor 594) following irradiation (10 Gy) after modulation of WRN expression. Nucleus was stained with DAPI (blue), and merged image of both is shown in the lower column. "Sec. control" is secondary antibody control (scale bar, 2 μm).

(D) Bar graph showing quantification of number of 53BP1 foci upon irradiation in case of WRN knockdown, overexpression, and knockdown followed by overexpression as compared with transfection control. A minimum of 100 cells were analyzed for each sample, 53BP1 foci counted and plotted as bar graph using GraphPad Prism 5 software depicting mean ± SEM (ns: not significant, *$p < 0.05$, **$p < 0.005$, ***$p < 0.0001$).

See also Figure S7.

higher oxidation and base alteration tendencies at telomeric sequences (G-rich), as compared with others (Oikawa and Kawanishi, 1999). Also, higher one-electron oxidation of a single 8-oxo-G when present in a G-quadruplex was observed, as compared with that in a duplex form (Szalai et al., 2002). In our study, experiments using piperidine treatment ruled out the possibility of a G-quadruplex structure harboring excessive modified bases post-irradiation. Thus, although individual guanine bases are the most sensitive to oxidative damage induced by IR, a 35-mer G-quadruplex structure exhibited lower oxidation sensitivity in our study. This is consistent with our data for IR-induced strand-breaks, and thus reiterates a structure-specific, but not sequence-specific, mechanism for the observed reduction in radiosensitivity. Few studies from the literature have shed light on the differential oxidation reactivity of the Guanine moiety when present in a G-quadruplex form, in comparison to that in a duplex form (Fleming and Burrows, 2013). In one of the studies, authors reported an extensive oxidation product profile for the human telomeric G-quadruplex structure, compared with a duplex DNA form, along with differential patterns of oxidation sensitivity within independent G4-DNA forms (hybrid, propeller, basket etc.) (Fleming and Burrows, 2013). Interestingly, they observed reduced base release upon sugar oxidation in G4-DNA (<10%), when compared with a duplex form (~20%), which is consistent with our current findings.

Previous studies have suggested bond strength difference between AT and GC pairs, as one of the plausible reasons underlying variation in radiation sensitivity at GC-rich sequences (Kaplan et al., 1964; Wu et al., 2012). Although GC-richness of the genome alone is not sufficient to influence radiosensitivity of an organism, a GC-rich DNA sequence will possess higher propensity of G4-forming motifs, as compared with an AT-rich one. Thus, our finding that G-quadruplex structures are much less sensitive to radiation provides a rational interpretation to the observed GC content bias in radioresistance. G-quadruplex structures have been shown to exist in several regions of the genome, contributing to a number of vital cellular processes (Hansel-Hertsch et al., 2017). In a genome context, analyses of independent irradiated human

genome sequence data revealed significant negative correlation between the number of G4s in each chromosome and the propensity of that chromosome to harbor DNA breaks. Transcriptome analysis coupled with evaluation of G4seq data revealed that in case of highly expressed genes, the unprotected regions harbored significantly lower number of G4-containing promoters (data not shown). Thus, our study reveals a G4-dependent bias in radiation damage of individual chromosomes, irrespective of their similarity in GC content (~42%). Consistent to this, we did not observe colocalization of G-quadruplex-specific antibody (BG4) and radiation-induced DNA breaks (γH2AX or 53BP1 foci). Direct analysis of several genomic regions by both semi-quantitative and real-time PCR further confirmed that most of the genomic regions that form G-quadruplex were insensitive to radiation. Hence, our data establish that radiation sensitivity to human genome is nonrandom and is dictated by DNA conformations.

Radiation Dose and Radiosensitivity Sensitivity of Biological Systems

Exposure to IR is encountered at different instances and at varying intensities. From a daily background radiation exposure of ~5 μSv, a range of doses are encountered during thoracic X-ray (~1 mSv), diagnostic CT (1–10 mSV), or radiotherapy against cancer (up to 100 Sv or Gy) (Lobrich and Jeggo, 2007). Previous studies estimated that exposure to 1 Gy of γ-radiation can induce ~1000 SSBs and 50–100 DSBs in a single cell (Mullenders et al., 2009). Thus, the extent of damage at different instances might vary according to the dose encountered. In the present study, we employed a wide range of radiation doses, from 2 Gy to 2 kGy, depending on the sensitivity of the technique under study. For example, although 2 Gy radiation dose was sufficient for detection of significant DDR repair foci within a cell, a dose of 100 Gy was indispensable in gel-based assays, to ascertain cleavage at every nucleotide, ensuring optimum sensitivity of the assay. Evaluating effect of radiation on genome-wide G4-forming regions using PCR-based approach necessitates the use of higher IR doses (0.5–2 kGy) to ensure strand-breakage at every ~200 nt. Thus, our findings reveal that reduced radiosensitivity of regions harboring G-quadruplex motifs, as assayed using various experimental strategies, will have implications at cellular level even at low radiation doses encountered by an organism.

G4 Structures at Telomeres Exhibit Reduced Sensitivity to Radiation

Among various genomic regions known to harbor G4 structures, telomeres is a well-established example, owing to the elevated GC content and single-stranded nature of the telomeric overhang (Bochman et al., 2012; Bryan and Baumann, 2011). Telomere dysfunction is a complex biological process that has been shown to occur due to a number of factors such as genome instability, senescence, DNA repair defects, improper functioning of telomerase, and aging (Hewitt et al., 2012; Jurk et al., 2014). The role of G-quadruplex structure in DNA end protection at the telomeres is well established (Bochman et al., 2012). However, DNA damage at this site is only one of the several factors that might contribute to overall telomere defects/dysfunction. Although DNA damage at telomeres has been investigated, it is quite challenging to address the end result of an IR-induced DNA break at telomeres in the absence of shelterin complex and compare it to the frequency of damage at a non-telomeric region in the chromosome. In an interesting study, Doksani and Lange reported activation of DDR at telomere-internal DSBs, as assessed using a Fok1 endonuclease-tagged TRF1 mediated system (Doksani and de Lange, 2016). The findings reveal that shelterin-mediated suppression of NHEJ, alt-NHEJ, or the HR pathway is not apparent at a telomere, when a DSB was generated internally, highlighting the possibility of active DDR in case of a strand-break even at telomeres. In our studies, we find that human telomeric repeat sequences are shielded from IR-induced DNA breaks when present on a single-stranded DNA or plasmid DNA. More importantly, absence of colocalization of DNA strand-breaks (γH2AX or p53BP1 foci) and G-quadruplex structures (FISH signals) at telomeric ends following irradiation of the cells confirm the above findings and reveal the role of G-quadruplex in radioprotection. Taken together, our data reveal that G4 structures formed at telomeres play a significant role in safeguarding the chromosome ends in cells against radiation-induced DNA strand-breaks. However, once induced, DNA damage at the telomeres is known to persist owing to the absence of DDR, mediated by the shelterin complex (de Lange, 2005; Hewitt et al., 2012).

Levels of G-Quadruplex Resolving Helicase; WRN Modulates Radiosensitivity in Cells

G-quadruplexes are dynamic structures that are well regulated inside cells by means of various stabilizing factors and resolving helicases. WRN, one of the RECQ family helicases, possesses 3′-5′ exonuclease, 3′-5′ helicase and single-strand DNA annealing activities (Huang et al., 2000; Orren et al., 1999). Previous studies have observed ATP-dependent and -independent helicase activities, thus unwinding secondary structures such as G-quadruplexes throughout the genome, including those at the telomeres, *in vivo* (Mendoza et al.,

2016). Our study revealed that WRN-mediated unwinding of these structures in cells resulted in elevated radiosensitivity, whereas knockdown of WRN or stabilization of G-quadruplexes led to a reduction in radiosensitivity. Thus, perturbation of G-quadruplex structures inside cells, either by stabilizing factors or by resolving helicases, modulates their susceptibility to radiation *in vivo*.

Further, WRN also plays important roles in various cellular processes such as DNA repair and replication, telomere maintenance, and transcription (Bernstein et al., 2010; Croteau et al., 2014). These functions are regulated by several factors such as post-translational modifications, protein-protein interactions, preferential activity of particular protein domains (helicase, in resolving G4-DNA vs. helicase and exonuclease, both, for DNA repair activity). Previous studies have observed modest increase in radiation sensitivity in the absence of WRN owing to reduced DSB repair (Saintigny et al., 2002). It is important to delineate the current observations of reduced damage induction upon WRN knockdown, immediately post-IR, as compared with other studies in literature, which assess DNA DSB repair efficiency and cell death after a significant time period post-IR (e.g., 9–15 days in this study) (Yannone et al., 2001). Decreased repair efficiency upon irradiation and subsequent cell death in the absence of WRN is well attributed to its role in DNA DSB repair and could be potentially distinct from its G-quadruplex resolving abilities in the cell. Our findings reveal that perturbation of G-quadruplex resolving helicases inside a cell can modulate the extent of IR-induced DNA damage induction. However, its effect on DNA repair and overall survival could be variable depending on the multi-faceted functions of the independent helicases.

Other Factors Contributing toward Radioprotection of Genome

It is presumed that sensitivity of a cell toward radiation is affected by a number of factors such as genome organization, nuclear microenvironment, hypoxia, DNA repair capacity, cell type, proliferation rate, and cell cycle phase. Polyamines such as spermine and spermidine, essential for growth and survival of mammalian cells, are well-studied scavengers of oxygen-radical species, which protect the genome against oxidative damage, and thus, are key mediators of cellular redox balance in a cell (Douki et al., 2000; Murray Stewart et al., 2018).

Influence of genome compartmentalization (euchromatin/heterochromatin) on sensitivity to IR-induced DNA damage and repair has been long debated in the field. Although some groups believe that heterochromatin is indeed less susceptible to IR-induced DNA damage as compared with euchromatin owing to DNA compaction, others report distinct differences in DDR and downstream repair between the two compartments (Chiolo et al., 2013; Falk et al., 2008; Lorkovic et al., 2017). Fascinating studies in eukaryotes have revealed differential DDR pattern in heterochromatin upon induction of IR-induced DNA damage, wherein induced DSBs are shifted away from heterochromatic regions before processing for repair (Chiolo et al., 2011; Ryu et al., 2015). Preliminary studies suggest that both heterochromatin and euchromatin regions showed susceptibility to IR, although cells that showed colocalization of DSB marker (53BP1) and euchromatin marker (AcH3K9) or heterochromatin marker (TIF1β) were seen less often (only ~7% of the cells; Figure S8). Although multiple factors affecting radiation sensitivity in a cell have been addressed previously, to our knowledge, this is the first report of a DNA secondary structure modulating IR-induced DNA damage.

Mechanism of G4-mediated Radioprotection and Its Impact on DNA Rearrangements

The findings presented here help to comprehend the plausible mechanism by which a quadruplex structure is protected by the action of radiation. Elegant experiments using flash photolysis and pulse radiolysis techniques, have revealed "hole trapping" property of a G-quartet structure (Figure 2E) (Choi et al., 2013; Lech et al., 2013; Wu et al., 2015). A single guanine residue possesses highest oxidation potential among the four nucleotides, whereas a G4 planar quartet displays low oxidation potential (Choi et al., 2013). Consistent with these observations, we observed selective susceptibility of the single-stranded loop sequence, as opposed to the resistant planar quartet in a G4 structure. Thus, the observed radioresistance of G-quartet structures can be well attributed to Hoogsteen hydrogen bonding between the guanine residues, as it may contribute to the differential radiosensitivity observed between a single guanine and that of a G-quadruplex structure (Figure 2E). Breakage at guanine in the single-stranded loop region reiterates the finding that structure of the DNA plays a vital role in imparting radioprotection to a G-quadruplex form of DNA. DNA strand-breaks are the primary requisites for genome rearrangements such as chromosomal translocations, inversions, and deletions. Our study establishes a GC-rich bias in protection of genomic sequences against radiation-induced breaks, making AT-rich sequences more prone to breakage, and subsequent rearrangements. For example, AT-rich Alu repeats have been shown to be involved in MLL rearrangements (Mani

and Chinnaiyan, 2010). Thus, our findings substantiate the observed sensitivity of AT-rich sequences toward radiation-induced DNA damage and rearrangements in the genome.

Differential Sensitivity of the Genome to IR: implications in Cellular Functions and Evolution

In addition to the skewed GC content in many radioresistant bacterial genomes, studies have also predicted a high number of G4-forming motifs in *Deinococcus radiodurans* (Kota et al., 2015). Considering this, it is easy to envisage a survival advantage gained by these bacteria, by virtue of G-quadruplexes in the genome, highlighting an important role of these structures in the evolution of radioresistance. Nonetheless, other factors such as elevated DNA repair, compaction of the genome, protection against oxidative stress etc., might contribute toward radioresistance in general, as is hypothesized in the famously AT-rich radioresistant organism, *Dictyostelium discoideum* (Deering, 1968).

Type and nature of DNA damage often dictates the repair pathway choice operating at the damaged site. Since our findings indicate an increased sensitivity of AT-rich sequences as opposed to GC-rich regions, we predict an AT sequence-biased evolution of DNA repair proteins operating in the cell, in order to maintain genomic integrity. Artemis, a versatile exonuclease and endonuclease involved in NHEJ has been shown to specifically resect AT-rich sequences but not those harboring GC (Chang et al., 2015). However, this needs to be investigated further. The findings presented here could also improve our understanding on the potential mechanism of radioresistance in cancer cells, which has important clinical implications. This information could be effectively harnessed for developing novel cancer treatment modalities, especially against radioresistant cancers.

Overall, this study establishes a paradigm shift in our understanding of the distribution of radiation-induced DNA breaks within the genome. We anticipate that our findings will help shed light on the evolution of GC content of an organism, regulation of multiple cellular processes, and differential radiation sensitivity among organisms.

Limitations of the Study

Since G-quadruplexes are highly dynamic and regulated structures, it is important to note that all the G-quadruplex-forming motifs analyzed in our study will not exist as secondary structures at a given time inside the cell. Since several experiments are based on population analysis, this caveat may not affect our interpretations. Considering that G4-forming motifs account for about 2% of whole genome, it may be interesting to investigate the role of flanking sequences and other non-B DNA structures such as Triplex and sticky DNA in conferring radioresistance. Further, detailed studies are required to understand the contribution of chromatin organization toward radiosensitivity of an organism.

METHODS

All methods can be found in the accompanying Transparent Methods supplemental file.

SUPPLEMENTAL INFORMATION

Supplemental Information can be found online at https://doi.org/10.1016/j.isci.2019.10.033.

ACKNOWLEDGMENTS

We thank Dr. Mridula Nambiar, Dr. Sagar Sengupta, Dr Utpal Nath, Dr. Robin Sebastian, Mr. Dipayan Ghosh, and other members of SCR laboratory for critical reading and comments on the manuscript. We thank Dr. Mrinal Srivastava and Ms. Shivangi Sharma for their help in cell culture. We also thank Dr. Shankar Balasubramanian for pSANG10-3F-BG4 plasmid construct. We thank Confocal, FACS, and Central Animal Facilities, shRNA core facility of IISc for their help. This work was supported by grants from DAE (21/01/2016-BRNS/35074), DBT (BT/PR13458/COE/34/33/2015), and IFCP (IFC/5203-4/2015/131), IISc-DBT partnership program (DBT/BF/PR/INS/2011-12/IISc) to SCR and DBT (BT/PR13616/GET119/9/2015-DBT), DST (SR/FST/LSI-536/2012-DST-FIST) to BC. NK, SK are supported by Junior Research fellowship (JRF) from IISc; SVV, SD by Senior Research fellowship (SRF) from IISc; VG by SRF from CSIR; SSD by JRF, DBT, India.

AUTHOR CONTRIBUTIONS

SCR and BC coordinated the study and provided the reagents; SCR, BC, SVV, NK, SD, and VG designed the experiments, interpreted results, and wrote the manuscript; NK, SVV, SD, SK, SSD, and VG conducted the experiments.

DECLARATION OF INTERESTS

The authors declare no competing financial interests.

Received: October 1, 2018
Revised: June 12, 2019
Accepted: October 16, 2019
Published: November 22, 2019

REFERENCES

Agrawal, P., Hatzakis, E., Guo, K., Carver, M., and Yang, D. (2013). Solution structure of the major G-quadruplex formed in the human VEGF promoter in K+: insights into loop interactions of the parallel G-quadruplexes. Nucleic Acids Res. *41*, 10584–10592.

Aguilera, A., and Garcia-Muse, T. (2013). Causes of genome instability. Annu. Rev. Genet. *47*, 1–32.

Balasubramanian, B., Pogozelski, W.K., and Tullius, T.D. (1998). DNA strand breaking by the hydroxyl radical is governed by the accessible surface areas of the hydrogen atoms of the DNA backbone. Proc. Natl. Acad. Sci. U S A *95*, 9738–9743.

Bernstein, K.A., Gangloff, S., and Rothstein, R. (2010). The RecQ DNA helicases in DNA repair. Annu. Rev. Genet. *44*, 393–417.

Biffi, G., Di Antonio, M., Tannahill, D., and Balasubramanian, S. (2014). Visualization and selective chemical targeting of RNA G-quadruplex structures in the cytoplasm of human cells. Nat. Chem. *6*, 75–80.

Biffi, G., Tannahill, D., McCafferty, J., and Balasubramanian, S. (2013). Quantitative visualization of DNA G-quadruplex structures in human cells. Nat. Chem. *5*, 182–186.

Bochman, M.L., Paeschke, K., and Zakian, V.A. (2012). DNA secondary structures: stability and function of G-quadruplex structures. Nat. Rev. Genet. *13*, 770–780.

Breen, A.P., and Murphy, J.A. (1995). Reactions of oxyl radicals with DNA. Free Radic. Biol. Med. *18*, 1033–1077.

Bryan, T.M., and Baumann, P. (2011). G-quadruplexes: from guanine gels to chemotherapeutics. Mol. Biotechnol. *49*, 198–208.

Burma, S., Chen, B.P., and Chen, D.J. (2006). Role of non-homologous end joining (NHEJ) in maintaining genomic integrity. DNA Repair (Amst.) *5*, 1042–1048.

Cadet, J., and Wagner, J.R. (2013). DNA base damage by reactive oxygen species, oxidizing agents, and UV radiation. Cold Spring Harb. Perspect. Biol. *5*, a012559.

Chambers, V.S., Marsico, G., Boutell, J.M., Di Antonio, M., Smith, G.P., and Balasubramanian, S. (2015). High-throughput sequencing of DNA G-quadruplex structures in the human genome. Nat. Biotechnol. *33*, 877–881.

Chang, H.H., Watanabe, G., and Lieber, M.R. (2015). Unifying the DNA end-processing roles of the artemis nuclease: Ku-dependent artemis resection at blunt DNA ends. J. Biol. Chem. *290*, 24036–24050.

Cheng, M.J., and Cao, Y.G. (2017). TMPYP4 exerted antitumor effects in human cervical cancer cells through activation of p38 mitogen-activated protein kinase. Biol. Res. *50*, 24.

Chiolo, I., Minoda, A., Colmenares, S.U., Polyzos, A., Costes, S.V., and Karpen, G.H. (2011). Double-strand breaks in heterochromatin move outside of a dynamic HP1a domain to complete recombinational repair. Cell *144*, 732–744.

Chiolo, I., Tang, J., Georgescu, W., and Costes, S.V. (2013). Nuclear dynamics of radiation-induced foci in euchromatin and heterochromatin. Mutat. Res. *750*, 56–66.

Choi, J., Park, J., Tanaka, A., Park, M.J., Jang, Y.J., Fujitsuka, M., Kim, S.K., and Majima, T. (2013). Hole trapping of G-quartets in a G-quadruplex. Angew. Chem. Int. Ed. *52*, 1134–1138.

Chu, W.K., and Hickson, I.D. (2009). RecQ helicases: multifunctional genome caretakers. Nat. Rev. Cancer *9*, 644–654.

Ciccia, A., and Elledge, S.J. (2010). The DNA damage response: making it safe to play with knives. Mol. Cell *40*, 179–204.

Cooke, M.S., Evans, M.D., Dizdaroglu, M., and Lunec, J. (2003). Oxidative DNA damage: mechanisms, mutation, and disease. FASEB J. *17*, 1195–1214.

Croteau, D.L., Popuri, V., Opresko, P.L., and Bohr, V.A. (2014). Human RecQ helicases in DNA repair, recombination, and replication. Annu. Rev. Biochem. *83*, 519–552.

Daly, M.J. (2009). A new perspective on radiation resistance based on Deinococcus radiodurans. Nat. Rev. Microbiol. *7*, 237–245.

Das, K., Srivastava, M., and Raghavan, S.C. (2016). GNG motifs can replace a GGG stretch during G-quadruplex formation in a context dependent manner. PLoS One *11*, e0158794.

de Lange, T. (2005). Shelterin: the protein complex that shapes and safeguards human telomeres. Genes Dev. *19*, 2100–2110.

Deering, R.A. (1968). Dictyostelium discoideum: a gamma-ray resistant organism. Science *162*, 1289–1290.

Doksani, Y., and de Lange, T. (2016). Telomere-internal double-strand breaks are repaired by homologous recombination and PARP1/Lig3-dependent end-joining. Cell Rep. *17*, 1646–1656.

Douki, T., Bretonniere, Y., and Cadet, J. (2000). Protection against radiation-induced degradation of DNA bases by polyamines. Radiat. Res. *153*, 29–35.

Falk, M., Lukasova, E., and Kozubek, S. (2008). Chromatin structure influences the sensitivity of DNA to gamma-radiation. Biochim. Biophys. Acta *1783*, 2398–2414.

Fleming, A.M., and Burrows, C.J. (2013). G-quadruplex folds of the human telomere sequence alter the site reactivity and reaction pathway of guanine oxidation compared to duplex DNA. Chem. Res. Toxicol. *26*, 593–607.

Hansel-Hertsch, R., Di Antonio, M., and Balasubramanian, S. (2017). DNA G-quadruplexes in the human genome: detection, functions and therapeutic potential. Nat. Rev. Mol. Cell Biol. *18*, 279–284.

Hewitt, G., Jurk, D., Marques, F.D., Correia-Melo, C., Hardy, T., Gackowska, A., Anderson, R., Taschuk, M., Mann, J., and Passos, J.F. (2012). Telomeres are favoured targets of a persistent DNA damage response in ageing and stress-induced senescence. Nat. Commun. *3*, 708.

Huang, S., Beresten, S., Li, B., Oshima, J., Ellis, N.A., and Campisi, J. (2000). Characterization of the human and mouse WRN 3′–>5′ exonuclease. Nucleic Acids Res. *28*, 2396–2405.

Jackson, S.P., and Bartek, J. (2009). The DNA-damage response in human biology and disease. Nature *461*, 1071–1078.

Jurk, D., Wilson, C., Passos, J.F., Oakley, F., Correia-Melo, C., Greaves, L., Saretzki, G., Fox, C., Lawless, C., Anderson, R., et al. (2014). Chronic

inflammation induces telomere dysfunction and accelerates ageing in mice. Nat. Commun. *2*, 4172.

Kaplan, H.S., Earle, J.D., and Howsden, F.L. (1964). The role of purine and pyrimidine bases and their analogues in radiation sensitivity. J. Cell Comp. Physiol. *64* (*Suppl 1*), 69–89.

Kasai, H., and Nishimura, S. (1984). Hydroxylation of deoxyguanosine at the C-8 position by ascorbic acid and other reducing agents. Nucleic Acids Res. *12*, 2137–2145.

Kikin, O., D'Antonio, L., and Bagga, P.S. (2006). QGRS Mapper: a web-based server for predicting G-quadruplexes in nucleotide sequences. Nucleic Acids Res. *34*, W676–W682.

Kota, S., Dhamodharan, V., Pradeepkumar, P.I., and Misra, H.S. (2015). G-quadruplex forming structural motifs in the genome of Deinococcus radiodurans and their regulatory roles in promoter functions. Appl. Microbiol. Biotechnol. *99*, 9761–9769.

Krisko, A., and Radman, M. (2013). Biology of extreme radiation resistance: the way of Deinococcus radiodurans. Cold Spring Harb. Perspect. Biol. *5*, a012765.

Lackner, D.H., Durocher, D., and Karlseder, J. (2011). A siRNA-based screen for genes involved in chromosome end protection. PLoS One *6*, e21407.

Lazzerini-Denchi, E., and Sfeir, A. (2016). Stop pulling my strings - what telomeres taught us about the DNA damage response. Nat. Rev. Mol. Cell Biol. *17*, 364–378.

Lech, C.J., Phan, A.T., Michel-Beyerle, M.E., and Voityuk, A.A. (2013). Electron-hole transfer in G-quadruplexes with different tetrad stacking geometries: a combined QM and MD study. J. Phys. Chem. B *117*, 9851–9856.

Lett, J.T. (1992). Damage to cellular DNA from particulate radiations, the efficacy of its processing and the radiosensitivity of mammalian cells. Emphasis on DNA double strand breaks and chromatin breaks. Radiat. Environ. Biophys. *31*, 257–277.

Lobrich, M., Cooper, P.K., and Rydberg, B. (1996). Non-random distribution of DNA double-strand breaks induced by particle irradiation. Int. J. Radiat. Biol. *70*, 493–503.

Lobrich, M., and Jeggo, P.A. (2007). The impact of a negligent G2/M checkpoint on genomic instability and cancer induction. Nat. Rev. Cancer *7*, 861–869.

Lomax, M.E., Folkes, L.K., and O'Neill, P. (2013). Biological consequences of radiation-induced DNA damage: relevance to radiotherapy. Clin. Oncol. (R Coll. Radiol.) *25*, 578–585.

Lorkovic, Z.J., Park, C., Goiser, M., Jiang, D., Kurzbauer, M.T., Schlogelhofer, P., and Berger, F. (2017). Compartmentalization of DNA damage response between heterochromatin and euchromatin is mediated by distinct H2A histone variants. Curr. Biol. *27*, 1192–1199.

Mani, R.S., and Chinnaiyan, A.M. (2010). Triggers for genomic rearrangements: insights into genomic, cellular and environmental influences. Nat. Rev. Genet. *11*, 819–829.

Mao, Z., Seluanov, A., Jiang, Y., and Gorbunova, V. (2007). TRF2 is required for repair of nontelomeric DNA double-strand breaks by homologous recombination. Proc. Natl. Acad. Sci. U S A *104*, 13068–13073.

Mendoza, O., Bourdoncle, A., Boule, J.B., Brosh, R.M., Jr., and Mergny, J.L. (2016). G-quadruplexes and helicases. Nucleic Acids Res. *44*, 1989–2006.

Mirkin, S.M. (2013). DNA replication: driving past four-stranded snags. Nature *497*, 449–450.

Mullenders, L., Atkinson, M., Paretzke, H., Sabatier, L., and Bouffler, S. (2009). Assessing cancer risks of low-dose radiation. Nat. Rev. Cancer *9*, 596–604.

Murray Stewart, T., Dunston, T.T., Woster, P.M., and Casero, R.A., Jr. (2018). Polyamine catabolism and oxidative damage. J. Biol. Chem. *293*, 18736–18745.

Nambiar, M., Goldsmith, G., Moorthy, B.T., Lieber, M.R., Joshi, M.V., Choudhary, B., Hosur, R.V., and Raghavan, S.C. (2011). Formation of a G-quadruplex at the BCL2 major breakpoint region of the t(14;18) translocation in follicular lymphoma. Nucleic Acids Res. *39*, 936–948.

Nambiar, M., Kari, V., and Raghavan, S.C. (2008). Chromosomal translocations in cancer. Biochim. Biophys. Acta *1786*, 139–152.

Nambiar, M., and Raghavan, S.C. (2011). How does DNA break during chromosomal translocations? Nucleic Acids Res. *39*, 5813–5825.

Nambiar, M., Srivastava, M., Gopalakrishnan, V., Sankaran, S.K., and Raghavan, S.C. (2013). G-quadruplex structures formed at the HOX11 breakpoint region contribute to its fragility during t(10;14) translocation in T-cell leukemia. Mol. Cell. Biol. *33*, 4266–4281.

Neidle, S., and Balasubramanian, S. (2006). Quadruplex Nucleic Acids. In RSC Biomolecular Sciences (RSC Biomolecular Sciences), pp. 1–252.

Nikiforov, Y.E., Koshoffer, A., Nikiforova, M., Stringer, J., and Fagin, J.A. (1999). Chromosomal breakpoint positions suggest a direct role for radiation in inducing illegitimate recombination between the ELE1 and RET genes in radiation-induced thyroid carcinomas. Oncogene *18*, 6330–6334.

Ohno, M., Miura, T., Furuichi, M., Tominaga, Y., Tsuchimoto, D., Sakumi, K., and Nakabeppu, Y. (2006). A genome-wide distribution of 8-oxoguanine correlates with the preferred regions for recombination and single nucleotide polymorphism in the human genome. Genome Res. *16*, 567–575.

Oikawa, S., and Kawanishi, S. (1999). Site-specific DNA damage at GGG sequence by oxidative stress may accelerate telomere shortening. FEBS Lett. *453*, 365–368.

Orren, D.K., Brosh, R.M., Jr., Nehlin, J.O., Machwe, A., Gray, M.D., and Bohr, V.A. (1999). Enzymatic and DNA binding properties of purified WRN protein: high affinity binding to single-stranded DNA but not to DNA damage induced by 4NQO. Nucleic Acids Res. *27*, 3557–3566.

Pang, D., Rodgers, J.E., Berman, B.L., Chasovskikh, S., and Dritschilo, A. (2005). Spatial distribution of radiation-induced double-strand breaks in plasmid DNA as resolved by atomic force microscopy. Radiat. Res. *164*, 755–765.

Pouget, J.P., Frelon, S., Ravanat, J.L., Testard, I., Odin, F., and Cadet, J. (2002). Formation of modified DNA bases in cells exposed either to gamma radiation or to high-LET particles. Radiat. Res. *157*, 589–595.

Puerto, S., Ramirez, M.J., Marcos, R., Creus, A., and Surralles, J. (2001). Radiation-induced chromosome aberrations in human euchromatic (17cen-p53) and heterochromatic (1cen-1q12) regions. Mutagenesis *16*, 291–296.

Raghavan, S.C., Swanson, P.C., Wu, X., Hsieh, C.L., and Lieber, M.R. (2004). A non-B-DNA structure at the Bcl-2 major breakpoint region is cleaved by the RAG complex. Nature *428*, 88–93.

Rodriguez, R., Miller, K.M., Forment, J.V., Bradshaw, C.R., Nikan, M., Britton, S., Oelschlaegel, T., Xhemalce, B., Balasubramanian, S., and Jackson, S.P. (2012). Small-molecule-induced DNA damage identifies alternative DNA structures in human genes. Nat. Chem. Biol. *8*, 301–310.

Ryu, T., Spatola, B., Delabaere, L., Bowlin, K., Hopp, H., Kunitake, R., Karpen, G.H., and Chiolo, I. (2015). Heterochromatic breaks move to the nuclear periphery to continue recombinational repair. Nat. Cell Biol. *17*, 1401–1411.

Saintigny, Y., Makienko, K., Swanson, C., Emond, M.J., and Monnat, R.J., Jr. (2002). Homologous recombination resolution defect in werner syndrome. Mol. Cell. Biol. *22*, 6971–6978.

Sancar, A., Lindsey-Boltz, L.A., Unsal-Kacmaz, K., and Linn, S. (2004). Molecular mechanisms of mammalian DNA repair and the DNA damage checkpoints. Annu. Rev. Biochem. *73*, 39–85.

Schiavone, D., Guilbaud, G., Murat, P., Papadopoulou, C., Sarkies, P., Prioleau, M.N., Balasubramanian, S., and Sale, J.E. (2014). Determinants of G quadruplex-induced epigenetic instability in REV1-deficient cells. EMBO J. *33*, 2507–2520.

Sinden, R. (1994). DNA Structure and Function (Academic Press), p. 398.

Spotheim-Maurizot, M., and Davidkova, M. (2011). Radiation damage to DNA in DNA-protein complexes. Mutat. Res. *711*, 41–48.

Steenken, S. (1997). Electron transfer in DNA? Competition by ultra-fast proton transfer? Biol. Chem. *378*, 1293–1297.

Steenken, S., and Jovanovic, S.V. (1997). How easily oxidizable is DNA? one-electron reduction potentials of adenosine and guanosine radicals in aqueous solution. J. Am. Chem. Soc. *119*, 617–618.

Sun, D., Guo, K., and Shin, Y.J. (2011). Evidence of the formation of G-quadruplex structures in the

promoter region of the human vascular endothelial growth factor gene. Nucleic Acids Res. *39*, 1256–1265.

Symington, L.S., and Gautier, J. (2011). Double-strand break end resection and repair pathway choice. Annu. Rev. Genet. *45*, 247–271.

Szalai, V.A., Singer, M.J., and Thorp, H.H. (2002). Site-specific probing of oxidative reactivity and telomerase function using 7,8-dihydro-8-oxoguanine in telomeric DNA. J. Am. Chem. Soc. *124*, 1625–1631.

Van Der Schans, G.P. (1978). Gamma-ray induced double-strand breaks in DNA resulting from randomly-inflicted single-strand breaks: temporal local denaturation, a new radiation phenomenon? Int. J. Radiat. Biol. Relat. Stud. Phys. Chem. Med. *33*, 105–120.

Vignard, J., Mirey, G., and Salles, B. (2013). Ionizing-radiation induced DNA double-strand breaks: a direct and indirect lighting up. Radiother. Oncol. *108*, 362–369.

Voloshin, O.N., Mirkin, S.M., Lyamichev, V.I., Belotserkovskii, B.P., and Frank-Kamenetskii, M.D. (1988). Chemical probing of homopurine-homopyrimidine mirror repeats in supercoiled DNA. Nature *333*, 475–476.

Wu, H., Zhang, Z., Hu, S., and Yu, J. (2012). On the molecular mechanism of GC content variation among eubacterial genomes. Biol. Direct *7*, 2.

Wong, H.M., Stegle, O., Rodgers, S., and Huppert, J.L. (2010). A toolbox for predicting g-quadruplex formation and stability. J. Nucleic Acids *2010*, 564946.

Wu, L., Liu, K., Jie, J., Song, D., and Su, H. (2015). Direct observation of guanine radical cation deprotonation in G-quadruplex DNA. J. Am. Chem. Soc. *137*, 259–266.

Yadav, V.K., Abraham, J.K., Mani, P., Kulshrestha, R., and Chowdhury, S. (2008). QuadBase: genome-wide database of G4 DNA–occurrence and conservation in human, chimpanzee, mouse and rat promoters and 146 microbes. Nucleic Acids Res. *36*, D381–D385.

Yannone, S.M., Roy, S., Chan, D.W., Murphy, M.B., Huang, S., Campisi, J., and Chen, D.J. (2001). Werner syndrome protein is regulated and phosphorylated by DNA-dependent protein kinase. J. Biol. Chem. *276*, 38242–38248.

Zhou, X., Liu, X., Zhang, X., Zhou, R., He, Y., Li, Q., Wang, Z., and Zhang, H. (2012). Non-randomized mtDNA damage after ionizing radiation via charge transport. Sci. Rep. *2*, 780.

ISCI, Volume *21*

Supplemental Information

G-quadruplex Structures Contribute to Differential Radiosensitivity of the Human Genome

Nitu Kumari, Supriya V. Vartak, Sumedha Dahal, Susmita Kumari, Sagar S. Desai, Vidya Gopalakrishnan, Bibha Choudhary, and Sathees C. Raghavan

Figure S1

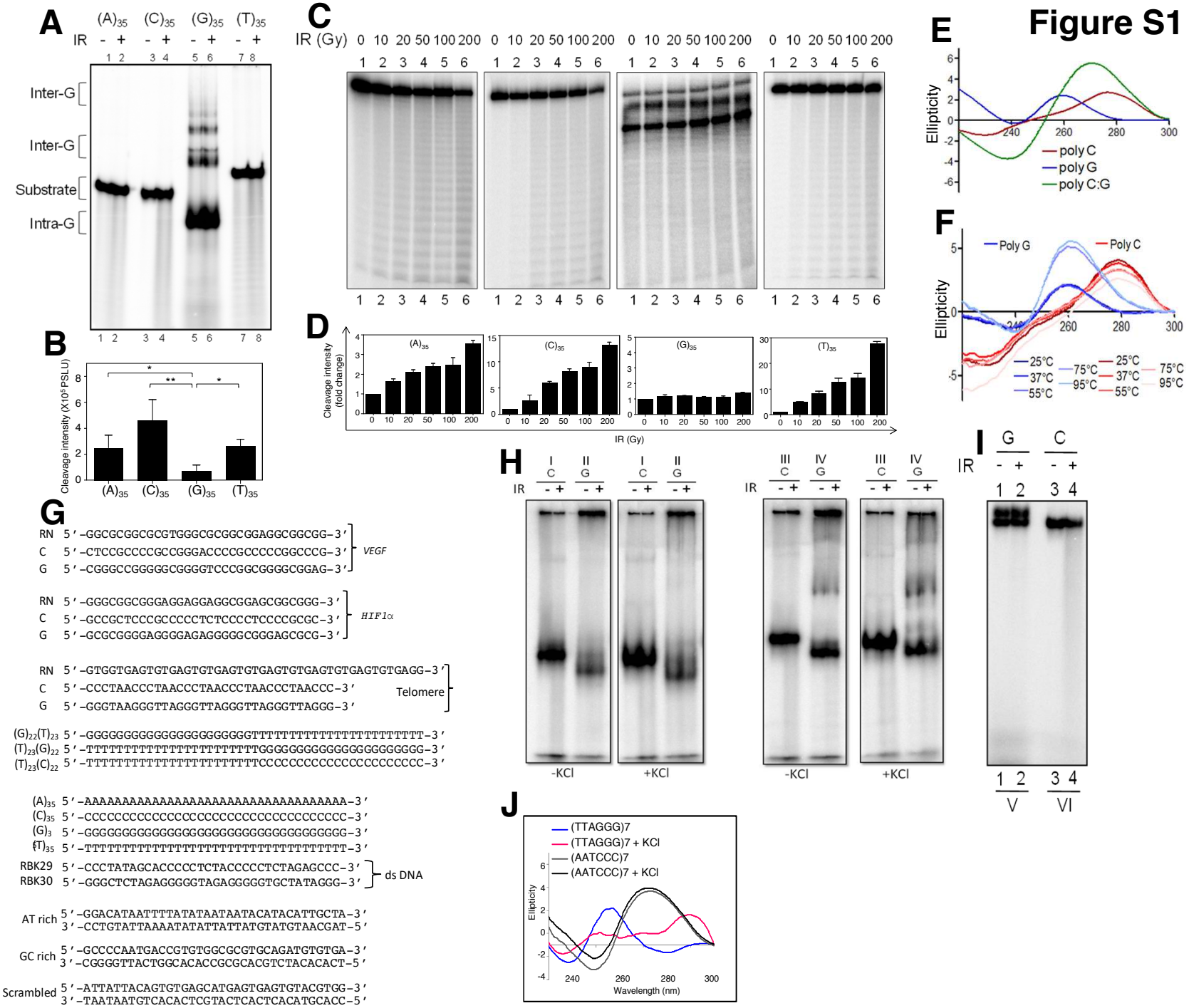
A
(A)35 (C)35 (G)35 (T)35
IR - + - + - + - +
1 2 3 4 5 6 7 8
Inter-G
Inter-G
Substrate
Intra-G
B
Cleavage intensity (X10^5 PSLU)
(A)35 (C)35 (G)35 (T)35
C
IR (Gy) 0 10 20 50 100 200
D
Cleavage intensity (fold change)
IR (Gy)
E
Ellipticity
poly C
poly G
poly C:G
F
Poly G
Poly C
Ellipticity
25°C 37°C 55°C 75°C 95°C
G
RN 5′-GGCGCGGCGCGTGGGCGCGGCGGAGGCGGCGG-3′
C 5′-CTCCGCCCCGCCGGGACCCCGCCCCCGGCCCG-3′
G 5′-CGGGCCGGGGGCGGGGTCCCGGCGGGGCGGAG-3′
VEGF
RN 5′-GGGCGGCGGGAGGAGGAGGCGGAGCGGCGGG-3′
C 5′-GCCGCTCCCGCCCCCTCTCCCCTCCCCGCGC-3′
G 5′-GCGCGGGGAGGGGAGAGGGGGCGGGAGCGCG-3′
HIF1α
RN 5′-GTGGTGAGTGTGAGTGTGAGTGTGAGTGTGAGTGTGAGTGTGAGG-3′
C 5′-CCCTAACCCTAACCCTAACCCTAACCCTAACCC-3′
G 5′-GGGTAAGGGTTAGGGTTAGGGTTAGGGTTAGGG-3′
Telomere
(G)22(T)23 5′-GGGGGGGGGGGGGGGGGGGGGGTTTTTTTTTTTTTTTTTTTTT-3′
(T)23(G)22 5′-TTTTTTTTTTTTTTTTTTTTTTTTGGGGGGGGGGGGGGGGGGGG-3′
(T)23(C)22 5′-TTTTTTTTTTTTTTTTTTTTTTTTCCCCCCCCCCCCCCCCCCCC-3′
(A)35 5′-AAAAAAAAAAAAAAAAAAAAAAAAAAAAAAAAAAA-3′
(C)35 5′-CCCCCCCCCCCCCCCCCCCCCCCCCCCCCCCCCCC-3′
(G)3 5′-GGGGGGGGGGGGGGGGGGGGGGGGGGGGGGGGGGG-3′
(T)35 5′-TTTTTTTTTTTTTTTTTTTTTTTTTTTTTTTTTTT-3′
RBK29 5′-CCCTATAGCACCCCCTCTACCCCCTCTAGAGCCC-3′
RBK30 5′-GGGCTCTAGAGGGGGTAGAGGGGGTGCTATAGGG-3′
ds DNA
AT rich 5′-GGACATAATTTTATATAATAATACATACATTGCTA-3′
3′-CCTGTATTAAAATATATTATTATGTATGTAACGAT-5′
GC rich 5′-GCCCCAATGACCGTGTGGCGCGTGCAGATGTGTGA-3′
3′-CGGGGTTACTGGCACACCGCGCACGTCTACACACT-5′
Scrambled 5′-ATTATTACAGTGTGAGCATGAGTGAGTGTACGTGG-3′
3′-TAATAATGTCACACTCGTACTCACTCACATGCACC-5′
H
I C II G III C IV G
IR - + - + - + - +
-KCl +KCl -KCl +KCl
I
G C
IR - + - +
1 2 3 4
1 2 V 3 4 VI
J
(TTAGGG)7
(TTAGGG)7 + KCl
(AATCCC)7
(AATCCC)7 + KCl
Ellipticity
Wavelength (nm)

Figure S1. Comparison of IR sensitivity in homopolymers of A, C, G and T and various DNA sequences that can fold into G4 DNA structures (Related to Figure 1). **A.** Native PAGE profile showing DNA fragmentation on homopolymeric A, C, G and T sequence, following irradiation (100 Gy). DNA substrates were irradiated and resolved on a 15% native gel. In each case, control substrates are denoted by -IR, while irradiated samples are denoted as +IR. Brackets indicate substrate in case of all four nucleotides. Slow and fast migrating species showing intermolecular (inter-G) and intramolecular (intra-G) quadruplex structures, respectively, have also been indicated. **B.** Quantification of cleavage intensity (observed as a smear), obtained from three independent repeats and plotted as a bar graph showing mean ± SEM (ns: not significant, *p < 0.05, **p < 0.005, ***p < 0.0001). **C.** Radiation-induced DNA strand-breaks when homopolymeric DNA (35 nt) of A, C, G and T sequence was exposed to increasing dose of IR. Oligomeric DNA was irradiated (0, 10, 20, 50, 100, 200 Gy), and resolved on a denaturing PAGE (15%). **D.** Each experiment was repeated a minimum of three times, the cleavage intensity was quantified using MultiGauge V3.0 and presented as a bar graph in the lower panel, showing mean ± SEM. **E.** Circular dichroism spectra of homopolymeric G, homopolymeric C and duplex C:G DNA acquired at 37^{o}C. The spectrum is plotted as a function of wavelength on the X-axis, and ellipticity values on the Y-axis **F.** Circular dichroism spectra of homopolymeric G and C sequences recorded at various temperatures (25, 37, 55, 75 and 95^{o}C). 35 mer poly Guanine (shades of blue) and poly Cytosine (shades of red) profiles are shown. The spectrum is plotted as a function of wavelength on the X-axis, and ellipticity values on the Y-axis. **G.** Oligomeric sequences of different DNA substrates used for the study. For each gene substrate, 'G' represents the G-quadruplex forming oligomer, 'C' represents its complementary region and 'RN' represents the random sequence of that particular region. Sequences used for homopolymeric A, C, G and T along with heteropolymeric (G22T23, T23G22 and T23C22) studies are also shown. Sequence of AT rich, GC rich and scrambled double-stranded DNA is also shown. **H-I.** Gel shift assay showing profiles of oligomers harboring G4 motifs from *VEGF* (I and II), *HIF1α* (III and IV) promoters (H) and telomeric region (I), upon irradiation. DNA substrates were exposed to 100 Gy IR, followed by resolution on Native PAGE (15%), in absence and presence of KCl in the gel. Corresponding complementary strands were used as controls and resolved in a similar manner. **J**. Circular dichroism spectra of oligomeric DNA harbouring human telomeric sequence. Spectrum for $(TTAGGG)_7$ in absence (blue) and presence of KCl (pink) has been shown, along with complementary control oligomers in grey (-KCl) and black (+KCl).

Figure S2

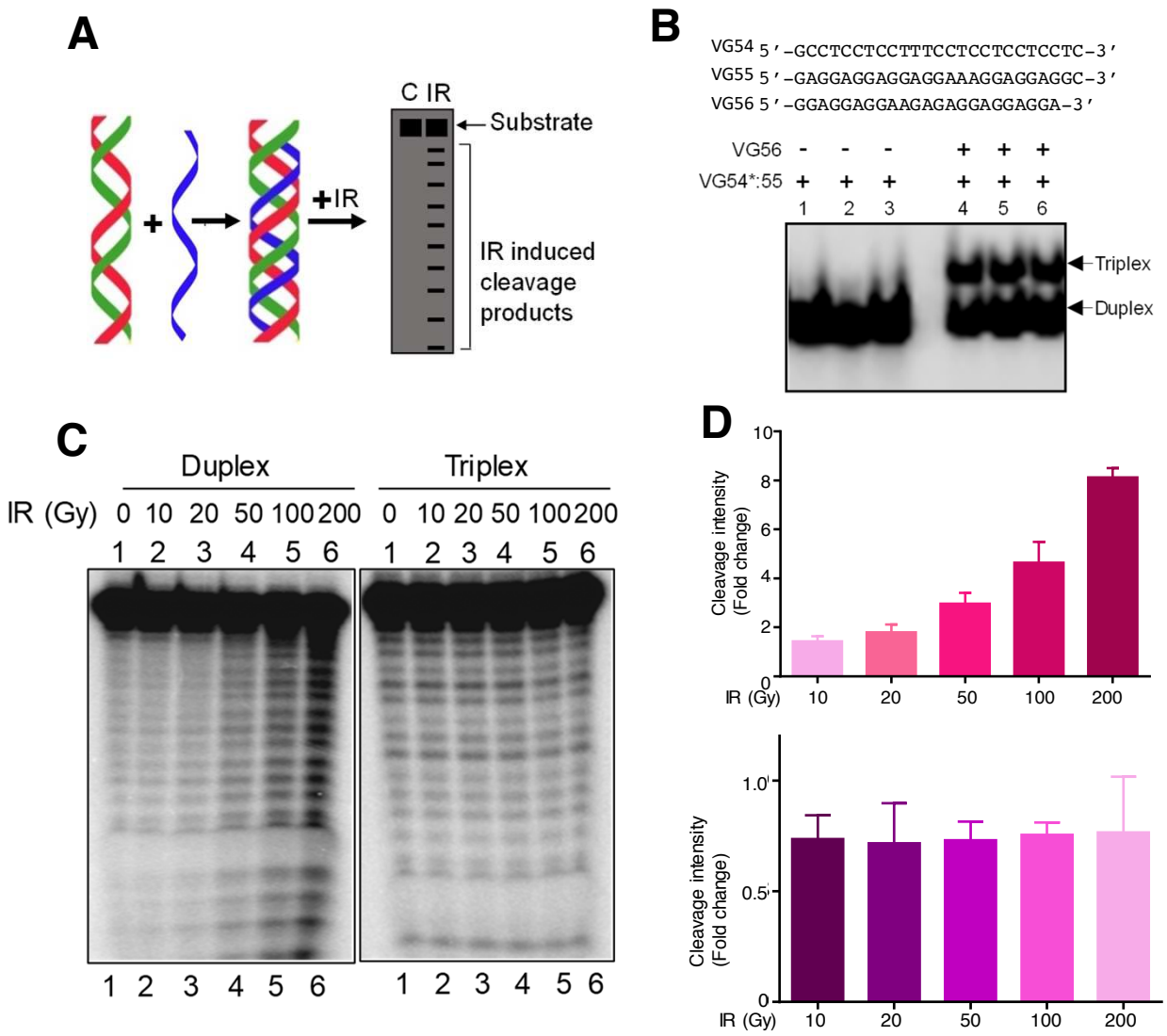
A
C IR
Substrate
+IR
IR induced cleavage products
B
VG54 5′-GCCTCCTCCTTTCCTCCTCCTCCTC-3′
VG55 5′-GAGGAGGAGGAGGAAAGGAGGAGGC-3′
VG56 5′-GGAGGAGGAAGAGAGGAGGAGGA-3′
VG56 - - - + + +
VG54*:55 + + + + + +
1 2 3 4 5 6
Triplex
Duplex
C
Duplex
Triplex
IR (Gy) 0 10 20 50 100 200 0 10 20 50 100 200
1 2 3 4 5 6 1 2 3 4 5 6
1 2 3 4 5 6 1 2 3 4 5 6
D
Cleavage intensity (Fold change)
IR (Gy) 10 20 50 100 200
Cleavage intensity (Fold change)
IR (Gy) 10 20 50 100 200

Figure S2. Comparison of IR sensitivity in oligomeric DNA that can fold into triplex DNA (Related to Figure 2)**. A.** Schematic representation of the assay employed for evaluation of IR-induced DNA strand breaks on triplex DNA structures. Radiolabeled VG54 was annealed with VG55 to form duplex DNA. Third strand, VG56 was then added and incubated at 37°C for 2 h in appropriate buffer to generate triplex DNA (A). **B.** Native PAGE profile showing formation of triplex DNA. Sequence of triplex forming oligomer used for the study is also shown. Lanes 1-3 indicates duplex DNA and lanes 4-6 is triplex DNA. **C.** Denaturing PAGE showing different forms of DNA, exposed to IR (10, 20, 50, 100 and 200 Gy), for analyzing the abundance of DNA breaks. **D.** Bar diagram showing quantification of IR induced cleavage on duplex and triplex DNA. In each case, the intensity of IR induced cleavage was subtracted from respective unirradiated control and plotted. Quantification of cleavage intensity, obtained from three independent repeats and plotted as a bar graph showing mean ± SEM.

Figure S3

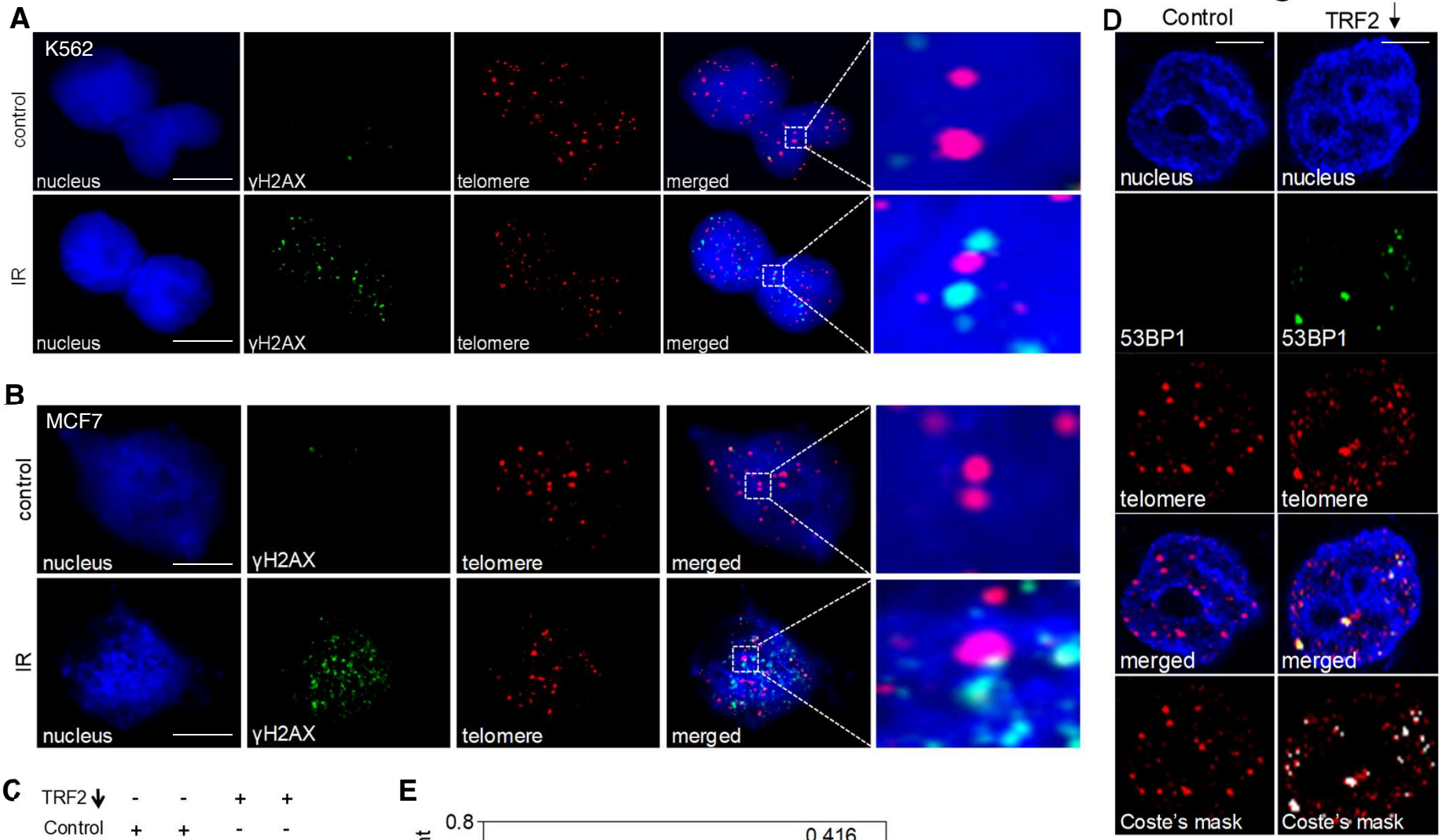
A
K562
control
IR
nucleus
γH2AX
telomere
merged
B
MCF7
C
TRF2
Control
IR
1
2
3
4
PCNA
Ponceau stained
D
Control
TRF2
53BP1
Coste's mask
E
Mander's coefficient
0.8
0.6
0.4
0.2
0.0
0.016
0.012
0.268
0.416
SCR
TRF2

Figure S3. Immunofluorescence and FISH analysis to investigate IR induced DSBs at telomere region in K562 and MCF7 cells (Related to Figure 3)**. A.** K562 cells were irradiated (10 Gy) and immunostained for γH2AX (FITC; green), followed by telomere FISH (Cy3; red). Nucleus was stained using DAPI (blue) and the merged image is shown as the extreme right panel (scale bar, 5 μm). **B.** IF- FISH analysis to investigate IR (10 Gy) induced DSBs at telomere region in MCF7 cells (scale bar, 5 μm). **C.** Representative western blot showing level of TRF2 in HeLa cells following its knockdown. A plasmid with scrambled sequence was used as control. Ponceau stained blot and level of PCNA served as loading control (scale bar, 5 μm). **D.** Representative IF-FISH images following knockdown for TRF2 in HeLa cells. Cells were transfected with either scrambled plasmid or TRF2 shRNA plasmid, and used for IF to detect 53BP1 foci (green; Alexa fluor 488). FISH was used to detect telomeres (red) and DAPI staining for nucleus (blue) (scale bar, 5 μm). **E.** Box-and-whiskers plots depicting Mander's colocalization coefficient (range: 0-1) as evaluated by JACoP plugin of ImageJ software. Experiment was performed in HeLa cells as described above, quantified and presented.

Figure S4

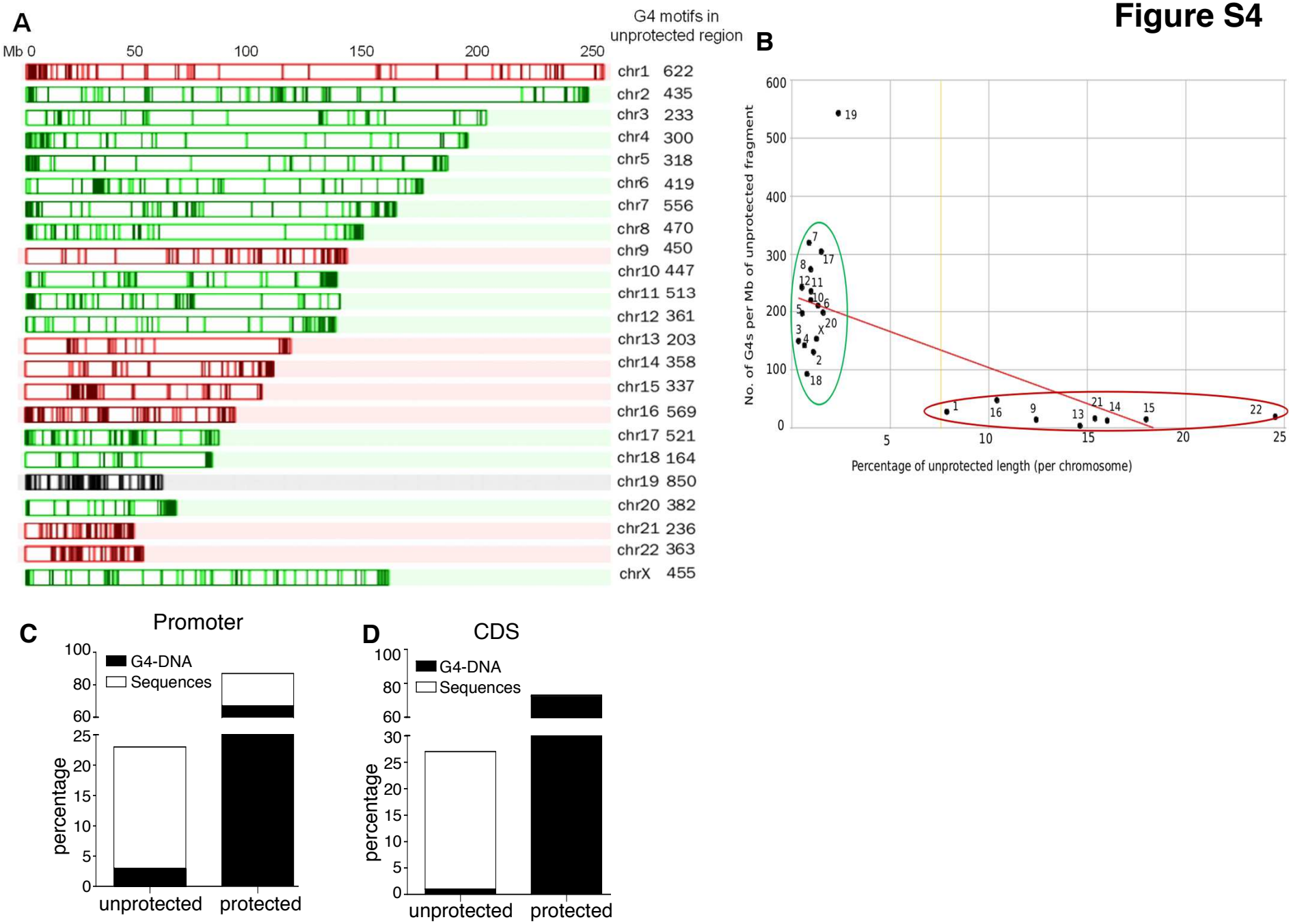
A
G4 motifs in unprotected region
Mb 0
50
100
150
200
250
chr1 622
chr2 435
chr3 233
chr4 300
chr5 318
chr6 419
chr7 556
chr8 470
chr9 450
chr10 447
chr11 513
chr12 361
chr13 203
chr14 358
chr15 337
chr16 569
chr17 521
chr18 164
chr19 850
chr20 382
chr21 236
chr22 363
chrX 455
B
No. of G4s per Mb of unprotected fragment
Percentage of unprotected length (per chromosome)
C
Promoter
G4-DNA
Sequences
percentage
unprotected
protected
D
CDS
G4-DNA
Sequences
percentage
unprotected
protected

Figure S4. Assessment of genome sequence in a human cell line for its sensitivity to IR in the context of G-quadruplex structures (Related to Figure 4)**. A.** Karyogram showing 1% damaged regions, wherein ones that are relatively less damaged are colored green and the ones that are relatively more damaged are colored red. The ones in black are outliers. **B.** A scatter plot depicting the inverse correlation between percentages of unprotected length in each chromosome vs. the number of G4 motifs per unprotected region. Higher number of G4 motifs correlates with less percentage of breakage and vice versa. The red cluster shows the chromosomes with higher number of G4 motifs and relatively less damage and the green cluster shows lower number of G4 motifs with relatively more damage. **C, D.** Histograms showing analysis of randomly selected genes for radiosensitivity (C). This is a representative set of 100 genes in which the promoter and the coding regions were assessed for G4 motifs. The graph in the right panel shows number of G4 motifs harbored by genes under study (D), both in the promoter and coding regions, which was high in the former case.

Figure S5

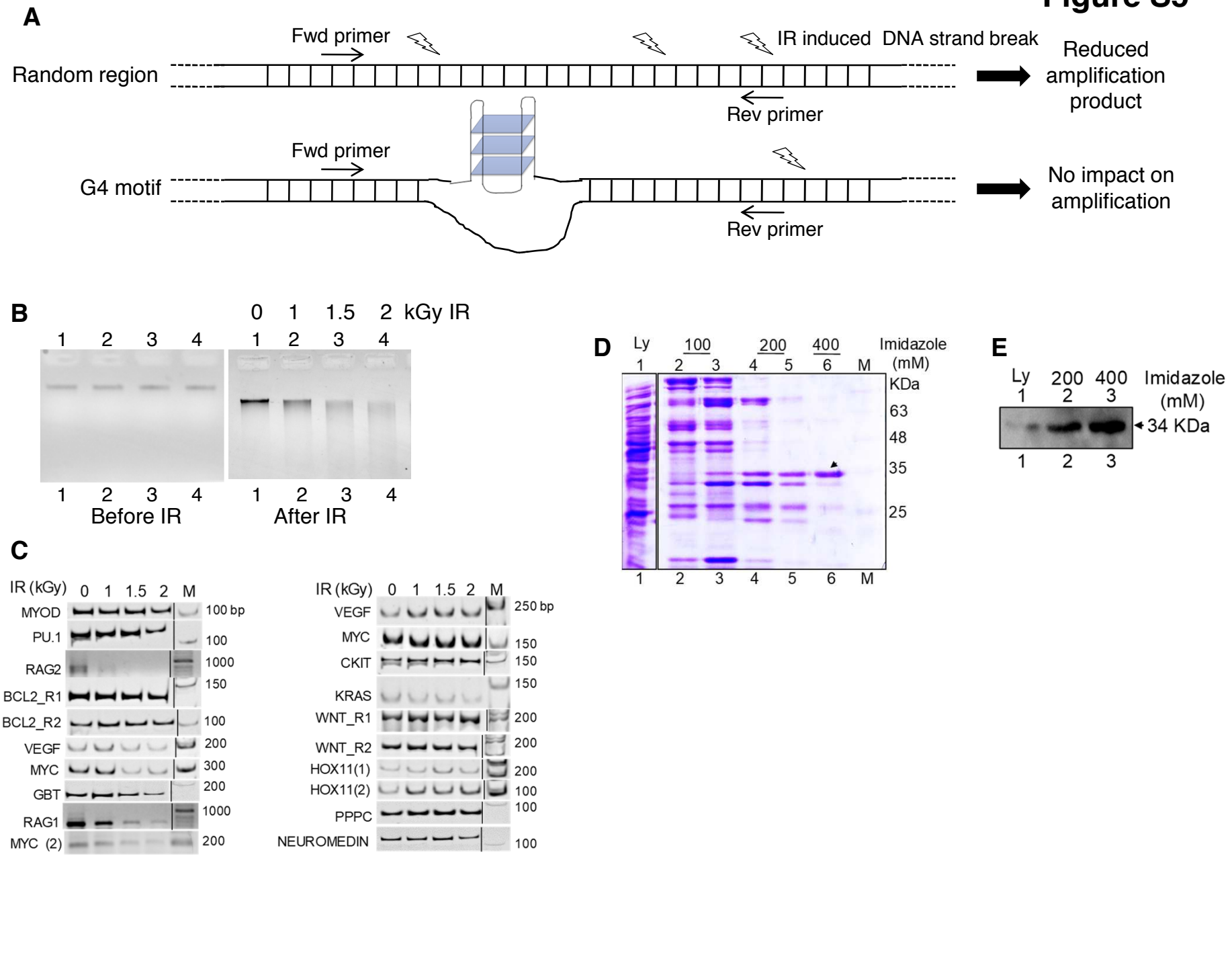
A
Fwd primer
IR induced DNA strand break
Random region
Reduced amplification product
Rev primer
Fwd primer
G4 motif
No impact on amplification
Rev primer
B
0 1 1.5 2 kGy IR
1 2 3 4
1 2 3 4
1 2 3 4
1 2 3 4
Before IR
After IR
C
IR (kGy) 0 1 1.5 2 M
MYOD
PU.1
RAG2
BCL2_R1
BCL2_R2
VEGF
MYC
GBT
RAG1
MYC (2)
100 bp
100
1000
150
100
200
300
200
1000
200
IR (kGy) 0 1 1.5 2 M
VEGF
MYC
CKIT
KRAS
WNT_R1
WNT_R2
HOX11(1)
HOX11(2)
PPPC
NEUROMEDIN
250 bp
150
150
150
200
200
200
100
100
100
D
Ly
100
200
400
Imidazole (mM)
1 2 3 4 5 6 M
KDa
63
48
35
25
1 2 3 4 5 6 M
E
Ly
200
400
Imidazole (mM)
1 2 3
34 KDa
1 2 3

Figure S5. Evaluation of randomly selected genes from human genome for their sensitivity to radiation (Related to Figures 5, 6)**. A.** Experimental strategy for detection of DNA strand-breaks upon irradiation in random regions of genome. Genomic DNA from Nalm6 cells was equalized and exposed to increasing dose of IR (1, 1.5 and 2 kGy), followed by amplification of various regions using specific forward and reverse primers. Twelve regions known to form G4 structures were amplified, along with appropriate random control regions and the DNA strand-break intensity was assessed using genomic PCR. Induction of DNA breaks in the template strand would lead to decreased amplification owing to the reduced template in the reaction, whereas an intact region would show no difference between the control and irradiated samples. **B.** Agarose gels showing equal genomic DNA in four samples before irradiation (left panel). The samples were exposed to increasing dose of IR (0, 1, 1.5 and 2 kGy) and resolved on an agarose gel (right panel). **C.** Gel profile showing genomic PCR products for control and irradiated samples (1, 1.5 and 2 kGy) for G4 forming regions, *VEGF, MYC, CKIT, KRAS, WNT*(1)*, WNT*(2)*, HOX11*(1)*, HOX11*(2)*, PPPC* and *NEUROMEDIN* (right panel), and regions devoid of G4 motifs, *MYOD, PU.1, RAG2, BCL2*(1)*, BCL2*(2)*, VEGF, MYC, GBT, RAG1* and *MYC*(2) (left panel). Molecular size marker is also shown. Vertical line indicates that image was cropped. Refer also Figure 5B. **D.** CBB gel profile showing purity of BG4 protein. Different concentrations (100-400 mM) of imidazole was used for the elution of BG4 protein that was bound to Ni-NTA column. Arrow indicates the band corresponding to the purified BG4. **E**. Western blotting to confirm the presence of BG4 protein by using anti-FLAG antibody. 'Ly' denotes total lysate.

Figure S6

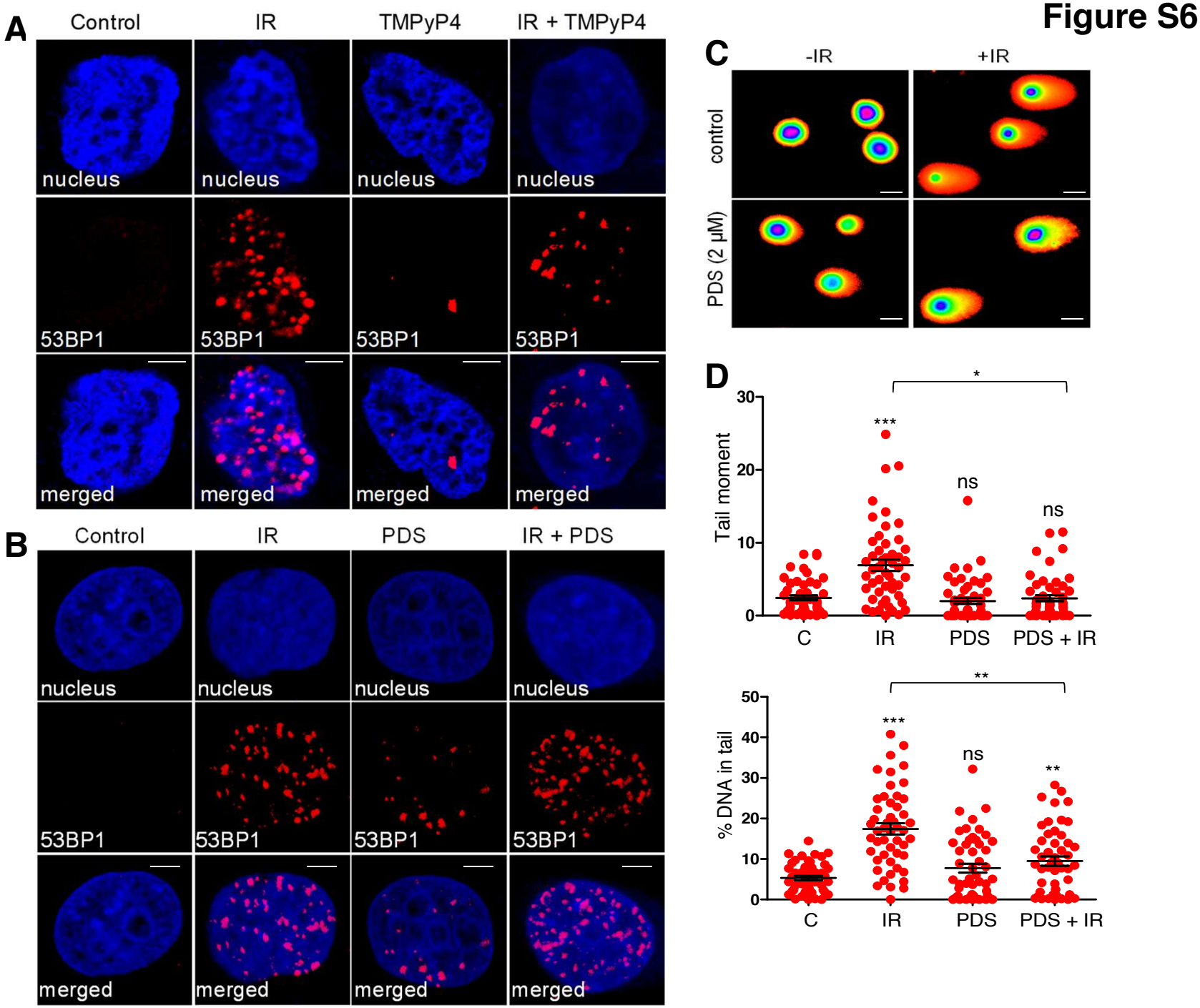
A
Control
IR
TMPyP4
IR + TMPyP4
nucleus
53BP1
merged
B
Control
IR
PDS
IR + PDS
nucleus
53BP1
merged
C
-IR
+IR
control
PDS (2 μM)
D
Tail moment
30
20
10
0
***
ns
ns
*
C
IR
PDS
PDS + IR
% DNA in tail
50
40
30
20
10
0
***
ns
**
**

Figure S6. Assessment of IR induced breaks following stabilization of G-quadruplex within the cells (Related to Figure 6)**. A.** Evaluation of DSBs following irradiation (10 Gy; 30 min recovery period) of MCF7 cells treated with a G4 stabilizing agent, TMPyP4 (5 μM, 5 h prior to irradiation). Cells alone, IR alone and TMPyP4 alone served as controls. In each case, 53BP1 foci (red, Alexa fluor 594), nucleus (blue, DAPI) and the merged image consisting of both the channels are shown (scale bar, 5 μm). **B.** Representative images showing the effect of pyridostatin (PDS) on radiation-induced DNA strand-break in HeLa cells (30 min post irradiation). Cells were treated with PDS (2 μM; 5 h), irradiated (10 Gy; 30 min recovery period) and processed for immunofluorescence as above (scale bar, 5 μm). **C, D.** Assessment of DNA breaks using comet assay, following treatment with G4 stabilizer PDS. Representative comet assay images showing control and irradiated (12 Gy; immediate harvesting) samples in presence of, pyridostatin (2 μM for 24 h), (scale bar, 10 μm) (C). Images were analyzed by using an automated software CometScore, and various parameters were calculated for each sample. Scatter plot showing quantitative parameters such as percentage DNA in tail and tail moment in each cell, and presented as mean ± SEM (D) (ns: not significant, *$p < 0.05$, **$p < 0.005$, ***$p < 0.0001$).

Figure S7

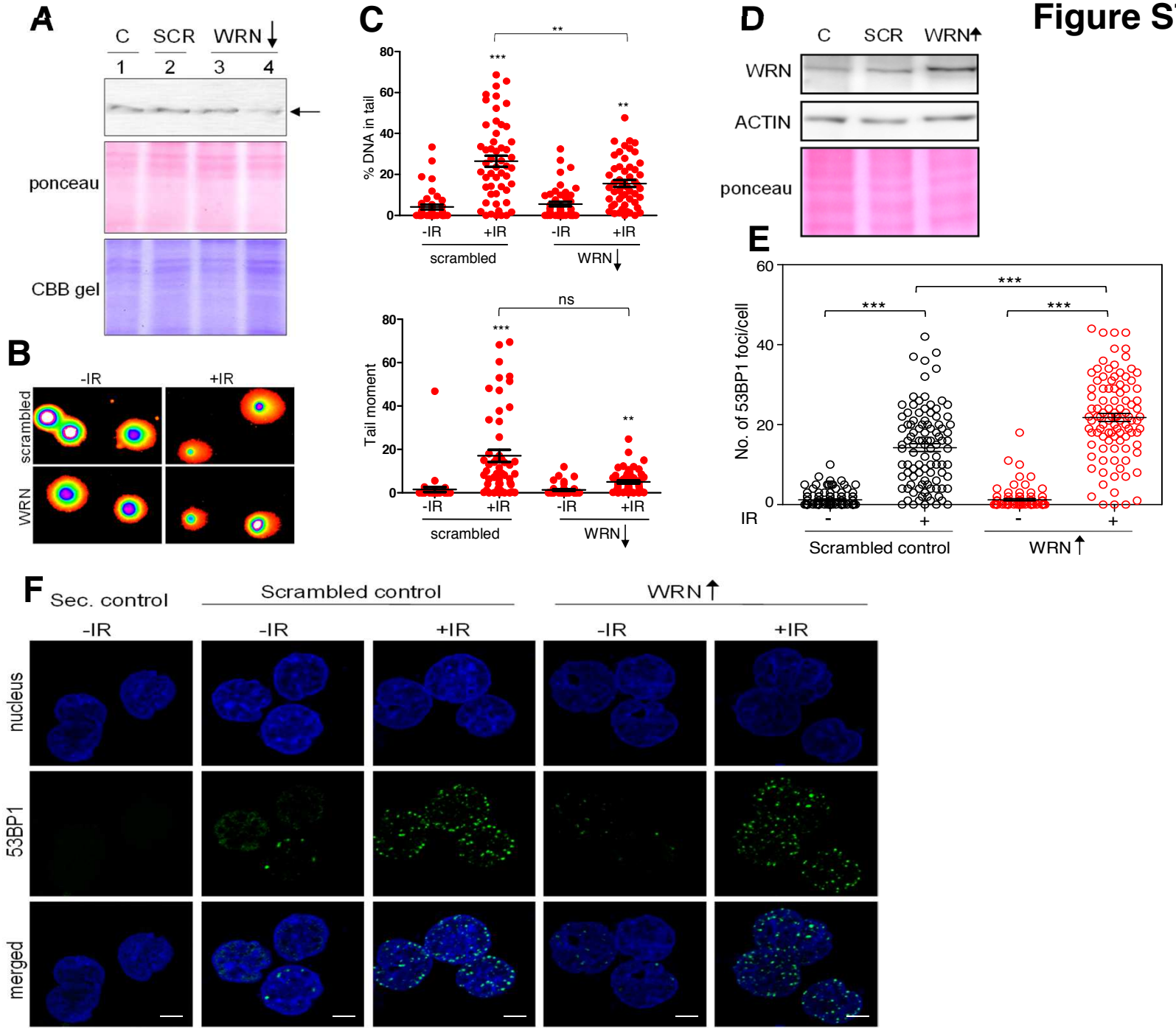
A
C
SCR
WRN
1
2
3
4
ponceau
CBB gel
B
-IR
+IR
scrambled
WRN
C
% DNA in tail
Tail moment
-IR
+IR
scrambled
WRN
ns
D
C
SCR
WRN
WRN
ACTIN
ponceau
E
No. of 53BP1 foci/cell
IR
Scrambled control
WRN
F
Sec. control
Scrambled control
WRN
-IR
+IR
nucleus
53BP1
merged

Figure S7. Evaluation of IR induced breaks following modulation of G-quadruplex formation within the cells by downregulation or upregulation of level of WRN (Related to Figure 7)**. A.** Representative western blot showing level of WRN helicase in Nalm6 cells upon transient transfection with WRN shRNA plasmids. A plasmid with scrambled sequence was used as control. Ponceau stained blot, and CBB stained gel reveal equal loading of samples. **B.** Images showing comet assay performed in cells following irradiation (10 Gy), after WRN knockdown (for 48 h) (scale bar, 10 μm). **C.** Scatter plot showing percentage DNA tail and tail moment for control and treated in knockdown samples. Comet images were analyzed using CometScore software as described above, and a scatter plot depicting mean ± SEM is shown (ns: not significant, *$p < 0.05$, **$p < 0.005$, ***$p < 0.0001$). **D.** Representative western blot showing overexpression of WRN helicase in Nalm6 cells. Actin and ponceau stained blot served as loading controls. 'C' refers to cells alone control, whereas 'SCR' denotes the scrambled plasmid control for transfection. **E**. Scatter plot showing quantification of number of 53BP1 foci upon irradiation following WRN overexpression, as compared to transfection control. A minimum of 100 cells were analyzed for each sample, 53BP1 foci counted and plotted as scatter plot using GraphPad Prism 5 software depicting mean ± SEM (ns: not significant, *$p < 0.05$, **$p < 0.005$, ***$p < 0.0001$). **F**. Representative immunofluorescence images showing 53BP1 foci formation (green) upon irradiation following WRN overexpression. Nucleus was stained with DAPI (blue), and merged image of both is shown in the lower column. Post transfection, cells were irradiated (10 Gy), allowed to recover for a period of 30 min (scale bar, 2 μm).

Figure S8

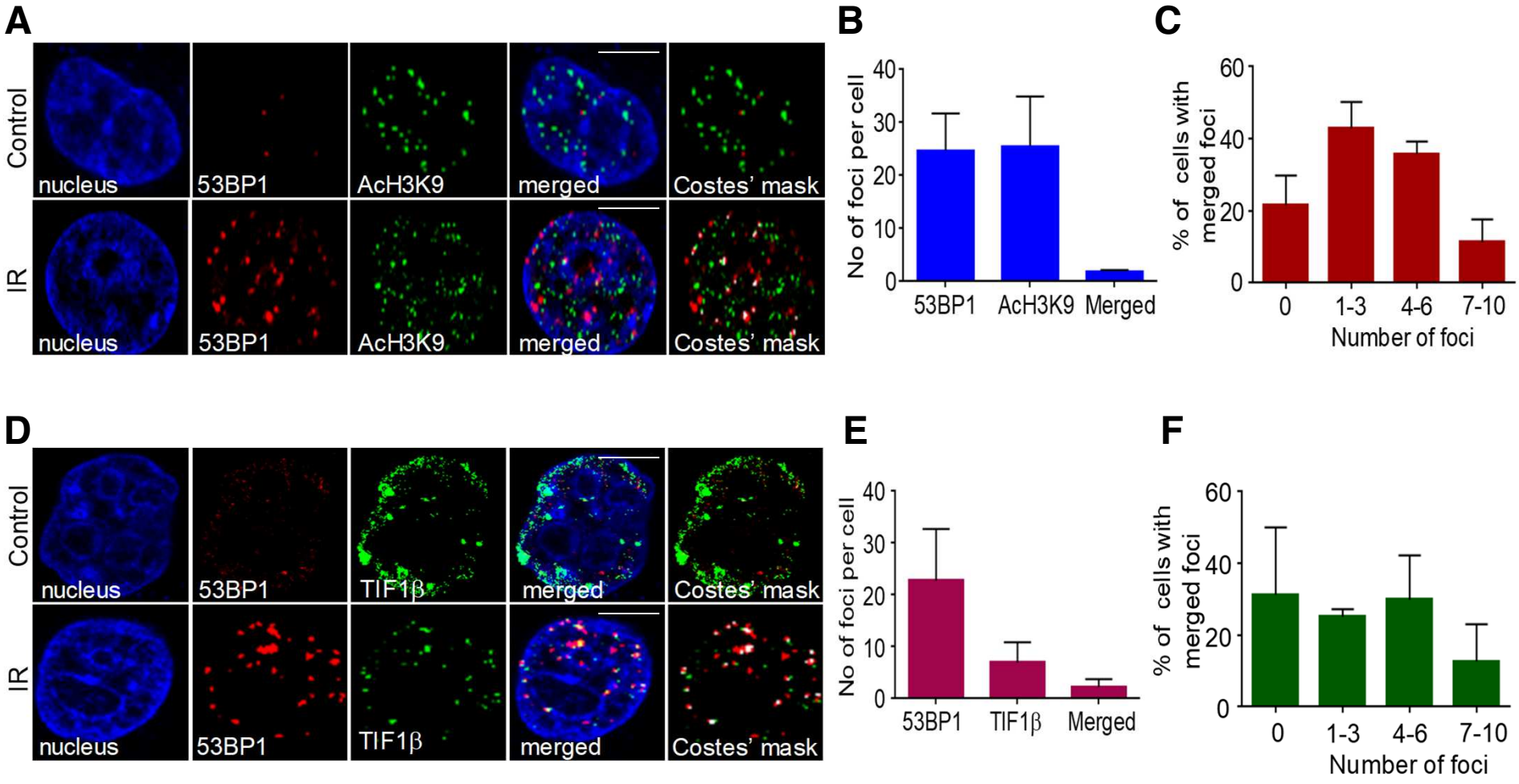
A
Control
IR
nucleus
53BP1
AcH3K9
merged
Costes' mask
B
No of foci per cell
40
30
20
10
0
53BP1
AcH3K9
Merged
C
% of cells with merged foci
60
40
20
0
0
1-3
4-6
7-10
Number of foci
D
Control
IR
nucleus
53BP1
TIF1β
merged
Costes' mask
E
No of foci per cell
40
30
20
10
0
53BP1
TIF1β
Merged
F
% of cells with merged foci
60
40
20
0
0
1-3
4-6
7-10
Number of foci

Figure S8. Immunofluorescence analysis to evaluate the role of chromatin organization on induction of DNA breaks by IR (Related to Figure 7)**. A.** Representative immunofluorescence images showing control and irradiated cells (10 Gy). Cells were stained for 53BP1 and euchromatin marker, acetylated histone H3K9 (scale bar, 5 μm). **B**. Bar graph showing average number of 53BP1, AcH3K9 and the merged foci per cell upon irradiation. **C.** Bar graph showing the distribution of colocalized foci of 53BP1 and AcH3K9 in cells following irradiation. **D.** Representative immunofluorescence images showing 53BP1 and heterochromatin marker (TIF1β) stained control and irradiated cells (10 Gy) (scale bar, 5 μm). **E.** Bar graph showing average number of 53BP1, TIF1β, and the merged foci per cell. **F.** Bar graph showing the distribution of colocalized foci of 53BP1 and TIF1β in individual cells. In panels B, C, E and F quantification is based on a minimum of two hundred cells in each case and plotted as a bar graph showing mean ± SEM.

TRANSPARENT METHODS

Oligomeric DNA

Oligomeric DNA used in the study were purchased from Sigma-Aldrich (St Louis, MO, USA) or IDT (San Jose, USA). The sequence of oligomers used were MS5, 5'-AAAAAAAAAAAAAAAAAAAAAAAAAAAAAAAA-3'; MS4, 5'-CCCCCCCCCCCCCCCC-CCCCCCCCCCCCCCCCCCCC-3'; MS9, 5'- GGGGGGGGGGGGGGGGGGGGGGGGGGGG-GGGGGGGG-3'; MS3, 5'-TTTTTTTTTTTTTTTTTTTTTTTTTTTTTTTT-3'; MN150, 5'-GCGCGAGGGAGGGGAGGGGAGGGGGAGAGGGAAACAGGCCACGTAAAGCAACTCTCTA AAGGCAGCGTC-3'; MN151, 5'-GCGCGAGGGAATAAATAATAGGGGGAGAGGGAAACAGG-CCACGTAAAGCAACTCTCTAAAGGCAGCGTC-3'; MN154, 5'-GCGCGACTAAATAAATAAT-AGACAGAGACTAAAACAGGCCACGTAAAGCAACTCTCTAA-AGGCAGCGTC-3'; MN117, 5'-GCGGAGCGAGCCGAGCGAGCGTGTGAGGTTGAGTGCGTTGAAACAGGCCACGTAAAGCA ACTCTCTAAAGGCAGCGTC-3'; SV10, 5'-GGGGGGGGGGGGGGGGGGGGGGGTTTTTTT-TTTTTTTTTTTTTTT-3'; SV11, 5'-TTTTTTTTTTTTTTTTTTTTTTTGGGGGGGGGGGGGGGG-GGGGGGG-3'; SV12, 5'-TTTTTTTTTTTTTTTTTTTTTTTCCCCCCCCCCCCCCCCCCCCCC-3'; SV25, 5'-GGGTTAGGGTTAGGGTTAGGGTTAGGGTTAGGG-3'; SV26, 5'-CCCTAACCCT-AACCCTAACCCTAACCCTAACCC-3'; SV27, 5'-GGGTTAGGGTTAGGGTTAGGGTTAGGGT-TAGGGTTAGGGTTAGGG-3'; SV28, 5'-CCCTAACCCTAACCCTAACCCTAACCCTAACCC-TAACCCTAACCC-3'; VG53, 5'-GTGGTGAGTGTGAGTGTGAGTGTGAGTGTG-AGTGTGAGTGTGAGG-3'; VG17, 5'-TATAAAATGATTCTATCTAGTCTGGGGGC-3'; KD49, 5'-CGGGCCGGGGGCGGGGTCCCGGCGGGGCGGAG-3'; KD50, 5'-CTCCGCCCCGCC-GGGACCCCGCCCCCGGCCCG-3'; VG49, 5'-GGCGCGGCGCGTGGGCGCGGCGGAGG-CGGCGG-3'; MN89, 5'-GCCGCTCCCG-CCCCCTCTCCCCTCCCCGCGC-3'; RT17, 5'-GCGCGGGGAGGGGAGAGGGGGCGG-GAGCGCG-3'; VG51, 5'-GGGCGGCGGGAGGA GGAGGCGGAGCGGCGGG-3';VG54, 5'-GCCTCCTCCTTTCCTCCTCCTCCTC-3'; VG55, 5'-GAGGAGGAGGAGGAAAGGAGGAGGC-3'; VG56, 5'-GGAGGAGGAAGAGAGGAGGAGGA-3'; AKN86 (Hp1) 5'-CGGGATCGGAGGGATACGAGCTCGTATCCCTTTGATCCCG-3'; AKN87 (Hp2), 5'-CGAGATCGGAGAGATAGAAAAAACTATCTCTCCGATCTCG-3'; AKN88 (Hp3), 5'-CGAGATCGGAGAGATAGCCCCCCCTATCTCTCCGATCTCG-3'; AKN89 (Hp4), 5'-CGAGA-TCGGAGAGATAGTTTTTTCTATCTCTCCGATCTCG-3'; AKN90 (Hp5), 5'-CGAGATCGGAG-AGATAGGGGGGGCTATCTCTCCGATCTCG-3'; VG60, 5'-GGGCTGGGTGGGTGC-TGTCAAGGGCTGGG-3'; BTM2, 5'-GAAGGAGGGCAGGAGGGCTCTGGGTGGGTCTGT-3'; MN38, 5'-GCGCGAGGGAGGGGAGGGGAGGGGGAGAGG-3'; MN45, 5'-AGAAGGGG-

GAGGGGAGGGAGAGAGGGGGCGCCG-3'; DR53, 5'-GTTTTGCCCGGGGTC-CCGGGCGCTTTGGGC-3'. SK9, 5'-GGACATAATTTTATATAATAATACATACATTGCTA-3'; SK10, 5'-TAGCAATGTATGTATTATTATATAAAATTATGTCC-3'; SK11, 5'-GCCCCAATGA-CCGTGTGGCGCGTGCAGATGTGTGA-3'; SK12, 5'-TCACACATCTGCACGCGCCA-CACGGTCATTGGGGC-3'; SK13, 5'-ATTATTACAGTGTGAGCATGAGTGAGTGTACGTGG-3'; SK14, 5'-CCACGTACACTCACTCATGCTCACACTGTAATAAT-3'; SV23, 5'-GGGTTAGGGTTAGGGTTAGGG-3'; SV24, 5'- CCCTAACCCTAACCCTAACCC-3'. Telomere probe sequence, 5'-Cy3/CCCTAACCC-TAACCCTAA-3'; centromere probe sequence, 5'-Cy3/ ATTCGTTGGAAACGGGA-3'. Telomere and centromere probes were from IDT, USA.

All oligomers were gel purified on 8-15% denaturing polyacrylamide gel. The purified substrates were then radiolabeled at 5' end using γ-^{32}P-ATP, and T4 polynucleotide kinase as described before (Nambiar and Raghavan, 2012).

Cell lines and culture

MCF7 (human breast cancer), HeLa (human cervical cancer), HEK293T (human embryonic kidney cells) and K562 (human chronic myelogenous leukemia) were purchased from National Centre for Cell Science, Pune, India. Nalm6 cells were from Dr. M. R. Lieber. Cells were cultured in RPMI 1640 or MEM medium supplemented with 15% fetal bovine serum (FBS), 100 µg/ml Penicillin, and 100 µg/ml streptomycin and incubated at 37^{o}C in a humidified atmosphere containing 5% CO_2 as described before (Srivastava et al., 2012).

Irradiation

Samples were irradiated at room temperature using a Cobalt-60 gamma irradiator (BI 2000, BRIT, India). The dose rate of the source at the time of usage was 0.91 Gy/min. IR dose employed in the study varied according to the sample and the experiment, and are specified in the respective assays.

Preparation of DNA substrates

Double stranded oligomeric DNA was prepared by annealing radiolabeled MS3 and MS4 with their complementary strand MS5 and MS9, respectively in presence of 100 mM NaCl and 1mM EDTA as described before (Kumar et al., 2010). AT rich, GC rich and scrambled oligomers were prepared by annealing SK9 and SK10, SK11 and SK12, SK13 and SK14, respectively. Double stranded DNA containing telomeric repeat sequences was prepared by annealing SV23 and SV24 (3 repeats, Telo A), SV25 and SV26 (5 repeats, Telo B), SV27 and SV28 (7 repeats, Telo C), respectively.

For preparation of triplex DNA (Rustighi et al., 2002), previously described oligomers were synthesized and used. Radiolabeled oligomer, VG54 (60 nM) was annealed with unlabelled VG55 (300 nM) in presence of 100 mM NaCl and 1 mM EDTA. Third strand oligomer, VG56 was then annealed to the duplex DNA (Wu et al., 2007) in 1x triplex buffer (10 mM Tris [pH 7.5], 100 mM NaCl, 10 mM $MgCl_2$ and 1% glycerol) for 2 h at 37°C.

Plasmid constructs

WRN helicase overexpression vector, pMM290 (Addgene plasmid # 46038) was a gift from Raymond Monnat (USA) (Swanson et al., 2004).

Plasmid isolation and purification

For each plasmid, after transformation, *Escherichia coli* were cultured in 500 ml of Luria broth (Hi Media, USA) for 18 h at 37°C. Isolation of plasmid DNA was performed by standard alkaline lysis method (denaturing method) and purified by cesium chloride-ethidium bromide density gradient centrifugation as described (Sambrook et al., 1989). Briefly, 5.1 g CsCl was dissolved in 4.0 ml TE. About 5 mg of isolated plasmid and 0.7 mg Ethidium Bromide were added to CsCl solution, vortexed and centrifuged using rotor TLA110 and Quick seal tubes (Beckman Coulter, USA) for 12 h, 72,000 rpm at 20°C. Following removal of ethidium bromide by butanol extraction, the plasmid DNA was precipitated with isopropanol and was washed in 70% alcohol. The pellet was dissolved in TE (pH 8.0).

IR-induced DNA breaks

For studying the effect of IR-induced DNA breaks, radiolabeled oligomers were irradiated (10, 20, 50, 100, 200 Gy) and resolved on either denaturing or native polyacrylamide gels. In case of triplex DNA, increasing doses of radiation (10, 20, 50, 100 and 200 Gy) was used. A single dose (100 Gy) was used for irradiation of hairpin DNA substrates (Hp1-Hp5). To study the effect of irradiation induced single stranded versus double-stranded breaks, ssDNA and dsDNA substrates were irradiated with a dose of 100 Gy. To study the effect of radiation on G-rich oligomers derived from different genomic regions, *VEGF*, *Hif1α* and telomere, KD49, RT17 and SV27, respectively were radiolabeled, incubated in TE buffer in presence or absence of KCl (Nambiar et al., 2011) and irradiated (150 Gy). Complementary C-rich oligomers (KD50, MN89 and SV28, respectively) and random oligomers (VG49, VG51 and VG53) derived from same genomic regions were also used for irradiation. In all cases, following irradiation, products were resolved either on 12-15% denaturing or native polyacrylamide gels. The gels were then dried, exposed to a screen, and signals were detected using a PhosphorImager (FLA9000, Fuji, Japan). In all experiments, unirradiated oligomeric DNA served as control. Quantification of the

IR-induced DNA cleavage was carried out using Multi Gauge V3.0, wherein the unirradiated control lane was subtracted from the irradiated ones.

Genomic DNA from Nalm6 cells was exposed to increasing dose of radiation (1, 1.5 and 2 kGy), followed by PCR amplification of the gene of interest using appropriate primers.

In case of IF-FISH experiments, cells were irradiated with a dose of 10 Gy, and incubated at 37^{o}C for a 30 min or 10 min recovery period, followed by harvesting and processing for immunofluorescence/FISH/comet assay. Radiation doses used for other experiments are indicated at appropriate figure legends.

Purification of BG4 protein

The plasmid expressing BG4 protein, pSANG10-3F-BG4 was a gift from Shankar Balasubramanian (Addgene plasmid # 55756). The plasmid was transformed into *E. coli*, BL21(DE3), and the culture was expanded by incubating at 30^{o}C, till the O.D. reached upto 0.6 (Biffi et al., 2013). The protein expression was then induced with 1 mM IPTG for a period of 16 h at 16^{o}C, harvested, and resuspended in lysis buffer (20 mM Tris-HCl [pH 8.0], 50 mM NaCl, 5% glycerol, 1% Triton X-100 and 1 mM PMSF). The cells were lysed by sonication, centrifuged, and the supernatant was then loaded onto a Ni-NTA chromatography column (Novagen). BG4 was eluted using increasing concentrations of Imidazole (100-400 mM), and purity was checked by CBB staining. BG4 enriched fractions were dialyzed against dialysis buffer (PBS containing 0.05% Triton X-100, 1 mM beta-mercaptoethanol, 5% glycerol and 0.1 mM PMSF) overnight at 4^{o}C. Identity of the protein was confirmed by immunoblotting, using an anti-FLAG antibody.

Circular dichroism (CD)

In order to assess G-quadruplex formation, DNA oligomers were subjected to CD spectroscopy at room temperature using a JASCO J-810 spectropolarimeter (50 nm/min scan speed, 10 cycle accumulations, 220-300 nm scan range) as described before (Nambiar et al., 2013; Raghavan et al., 2005). DNA of interest [ss DNA, ds DNA were resuspended in TE buffer, either in the presence or absence of 100 mM KCl or LiCl at 37^{o}C for 1 h, followed by CD spectroscopy measurements. The spectrum for buffer alone was subtracted from the experimental spectra. The ellipticity was obtained using the Spectra Manager software and was plotted as a function of wavelength. For annealing of double stranded DNA, equimolar concentrations of MS4 and MS9 were boiled in presence of 100 mM NaCl and 1 mM EDTA for 10 min and allowed to anneal by slow cooling.

Gel Mobility Shift Assay

Radiolabeled oligomers were incubated in the presence of 100 mM KCl for 1 h at 37°C, followed by irradiation as described before (Nambiar et al., 2011; Nambiar et al., 2013). The oligomers were then resolved on 12-15% native polyacrylamide gels, run at 150 V at room temperature, in the presence of KCl in the gel as well as the running buffer. The gels were dried, exposed to a PhosphorImager screen, and the signals were detected using a PhosporImager FLA9000 (Fuji, Japan).

Triplex DNA was prepared as described above by annealing radiolabeled VG54 with VG55 in presence of 100 mM NaCl and 1 mM EDTA. Annealed dsDNA was then incubated with triplex forming oligomer, VG56 in appropriate buffer (1 mM Tris [pH 7.5], 10 mM NaCl, 1 mM $MgCl_2$ and 1 % glycerol) for 2 h at 37°C. The oligomers were then resolved on 12% native polyacrylamide gels, (100 V at room temperature), in the presence of 100 mM $MgCl_2$ in 1x Tris Borate (pH 7.8) running buffer and radioactive signals were detected as described above.

DMS protection assay

Radiolabeled oligomers were incubated with 100 mM KCl (wherever indicated) at 37°C for 1 h, followed by irradiation (100 Gy). 1 µl DMS (1:10 stock) was added to the 10 µl reaction mixture and incubated at room temperature for 15 min, as described before (Das et al., 2016; Nambiar et al., 2011). Equal volume of piperidine (1:10 stock) was then added and the samples were heated for 30 min at 90°C. DNA was purified, loaded onto an 18% denaturing polyacrylamide gel, followed by drying, and subsequent visualization of the bands as described above.

The oligomers derived from BCL2 major breakpoint region (BTM2) (Nambiar et al., 2011), Region I (MN38) and II (MN45) of the HOX11 breakpoint region (Nambiar et al., 2013), BU1A (VG60) (Schiavone et al., 2014) and human telomeric region (SV27) were used for the study. Oligomeric DNA containing a random sequence, VG17 was also used for the study.

Immunocytochemistry

Cells were cultured on coverslips (50,000/ml for 24 h), irradiated (10 Gy), and allowed to recover for a period of 30 min at 37°C. Control cells (without IR) were sham treated, and processed in a similar way. After the recovery period, cells were harvested, washed with phosphate buffered saline (PBS) and fixed using 2% paraformaldehyde, PFA (10 min at room temperature), as described before (John et al., 2015; Sebastian and Raghavan, 2016). Following fixing, cells were permeabilized using PBS + 0.1% Triton X-100 (5-10 min at RT), blocked using PBST + 0.1% BSA + 10% FBS (1 h at 4°C), and incubated with appropriate primary antibodies, γ-H2AX (Cell Signaling Technology, USA), pATM, 53BP1, TRF2, TIF1β,

AcH3K9 (Santa Cruz Biotechnology, USA) at 4ºC overnight. Corresponding Alexa Fluor conjugated with secondary antibodies (Life Technologies, USA) were added and the cells were incubated at 4ºC for 2 h. Following antibody staining, the coverslip was mounted using DAPI, diazobicyclo[2.2.2]octane (DABCO) mix. Images were captured using Laser Confocal microscope (Zeiss, Germany, Olympus, FLUOVIEW FV3000, Japan) or Apotome Fluorescence Microscope (Zeiss, Germany).

For BG4 and γH2AX colocalization studies, HeLa or MCF7 cells were irradiated (10 Gy) and used for immunofluorescence as described above. Besides, a radiation dose titration (5, 10 and 20 Gy) was also performed in HeLa cells. In case of BG4, anti-FLAG was used for detection.

When required, images were analyzed for colocalization of signals by using the JACoP plugin of the ImageJ software, as described previously (Bolte and Cordelieres, 2006; Kumar et al., 2010). Mander's colocalization coefficient, which denotes the fraction of overlap of one color over the other, was chosen as one of the parameters of analysis. The value obtained for each cell was plotted in the form of a box and whisker plot, denoting mean ± SEM.

IF-FISH

Cells (MCF7, K562 and HeLa) were seeded, irradiated and processed for immunocytochemistry, as described above. Following IF, FISH was performed as described previously, with minor modifications (Dimitrova et al., 2008). Briefly, the cells were fixed post-IF using 2% PFA (2 min) followed by RNase A treatment (0.1 mg/ml; 1 h at 37ºC). The sample was washed twice with 2XSSC, once with distilled water and incubated with trypsin (5%) for 4 min at 37ºC. The sample was fixed again (2% PFA, 2 min, RT), followed by serial dehydration in 70, 90 and 100% ethanol (5 min each). Following air drying, the sample was denatured (85ºC for 5 min), incubated with the telomere or centromere probes (IDT, USA) for 10 min at 85ºC, and allowed to hybridize at room temperature (2 h). The coverslip was then mounted using DAPI:DABCO mix.

IF-FISH was also performed following knockdown of TRF2 in HeLa cells. For this, cells growing in log phase ($5x10^5$ cells) were transfected with shRNA plasmid (9 µg) that can target TRF2 (TRCN0000004811, shRNA core facility of IISc) using polyethylenimine method (Iyer et al., 2016). Cells were harvested after 24 h of incubation (37ºC) and TRF2 expression level was assessed by western blotting. For investigating the radiation induced DNA breaks, following TRF2 knockdown, cells were irradiated (10 Gy), allowed to recover for 30 minutes. Irradiated

cells were then subjected to immunofluorescence for detection of 53BP1 foci, following which IF-FISH was performed as described above.

In all cases, images were analyzed for colocalization of signals by using the JACoP plugin of the ImageJ software, as described previously (Bolte and Cordelieres, 2006; Kumar et al., 2010). Mander's colocalization coefficient, which denotes the fraction of overlap of one color over the other, was chosen as one of the parameters of analysis. The value obtained for each cell was plotted in the form of a box and whisker plot, denoting mean ± SEM.

Genomic DNA Extraction

Genomic DNA was extracted from Nalm6 cells, as described before (Nambiar and Raghavan, 2010; Raghavan et al., 2004). Briefly, cells were lysed with extraction buffer in the presence of Proteinase K (overnight at 37^{o}C) and genomic DNA was purified following phenol-chloroform extraction. DNA was resuspended in TE buffer and stored at 4^{o}C until use.

Real time PCR of irradiated genomic DNA

Genomic DNA was irradiated using gamma rays (1, 1.5 and 2 kGy) after resuspending in TE. Real time PCR was performed on irradiated genomic DNA samples in a BioRad IQ5 Real time PCR Detection System Ver2.1. Unirradiated DNA served as the control. Briefly, 10 ng of genomic DNA, 5 µl of 2x SYBR Green master mix containing dNTPs, $MgCl_2$ and Taq DNA Polymerase (Takara Bio Inc.) and 500 nM each of the respective forward and reverse primer were mixed in a total reaction volume of 10 µl. The reaction was run at 95^{o}C for 3 min, followed by 35 cycles of 95^{o}C for 30 sec, 58^{o}C for 30 sec and 72^{o}C for 30 sec. All PCRs were performed in triplicates. Ct values for respective control and irradiated samples were determined using Bio-Rad IQ5 analysis software.

Real time PCR primers used for the study were SV42, 5'-TGGGGGAGCGTGTCAGAAT-3', SV43, 5'-GCTTTAATTGTGTGATTGGAC-3' for *VEGF* G4, SV50, 5'-AGTTCCCTGGCAACATCTG-3', SV51, 5'-AATTTGGCACCAAGTTTGT-3' for VEGF random, SV46, 5'-GGAGGAGCAGCAGAGAAAG-3', SV47, 5'- GTGGGGAGGGTGGGGAAGGT-3' for *MYC* G4, SV52, 5'-TAGGCTGGAGGTCGTGGTTA-3', SV53, 5'-CGGCGCTTTCGGATTAACT-3' for *MYC* random, SV48, 5'- AGCAAGTAGTAATTGATGG-3', SV49, 5'-GCAAATACACAAAGAAAGC-3' for *KRAS* G4, SV54, 5'-ACACAGTCCAGACACTCTGC-3', SV55, 5'-ACGTGCAGAAACTCCTTGTTC-3' for *WNT* G4 region 1, SV56, 5'-CCAGCGCCGCAACTATAAGA-3', SV57, 5'-GGCGACTTTGGTTGTTGCCC- 3' for *WNT* G4 region 2, SV60, 5'-TAAGGCACTTTCTGGGCAGT-3', SV61, 5'-CTGCCAACCCCAGTAATGAT-3' for *CKIT* G4, SV66, 5'-GCAGGATAGCAGCACAGGATT-3',

SV67, 5’-GGCCTCAGGGAACAGAATGAT-3’ for BCL2 random region 2, SV58, MN34, 5' TTAAGCCTCGCCTTGTTC-3', MN35, 5'- CGGTGCAAGAGAGCTTCG-3' for HOX11, 5’-CAGTCTTCAGGCAAAACGTCGA-3’, SV59, 5’-TGGTCGGATTTCCAAAGACA-3’ for BCL2 random region 1, SV68, 5’-CCTCTTTCGGTCCCTCTTTC-3’, SV69, 5’-ATGGGTAGAGCGGCTGTAGA-3’ for MYOD random region, SV70, 5’-TGGTGGATAGGCAAGAAAGG-3’, SV71, 5’-ATCCCTAGGGCTCTGTTTCC-3’ for PU.1 random region, SV80, 5'-AAAACAACTTCCACAGTCCT-3', SV81, 5'-CAAGCTGGTTACGCCCCAGA-3' for PPPC G4, SV86, 5'-GCCCCGCGTTCTCCG-3', SV87, 5'-ACACACTCGGCCATTACGG-3' for USLP-1 G4, SV90, 5'-AACGGCCTCGGAGAAGTAAC-3', SV91, 5'-TGGCGCATTCGACCCAAATA-3' for NEUROMEDIN G4, SV92, 5'-GTCGGACTCCTACCCCTTTTG-3', SV93, 5'-CTGGTTTAACAGGCGTTCCC-3' for CALNEXIN G4, SV94, 5'-GGTCTTGTTCCTAAGGGGGC-3', SV95, 5'-TTTGACTGCGTGTTGTGCAG-3' for MYC random region 1, SV100, 5'-GGAATCCACCTCTTGAAGGCA-3', SV101, 5'-CTCCGCTCTGACCCAAGAAC-3' for GBT1 random region, SV104, 5'-AAGCTGGGGCTTATACTGACTG-3', SV105, 5'-GAGAGTTTGCTGGGGCACTG-3' for RAG1 random region, SV106, 5'-ACCCTCGTAGCTCGCACTTA-3', SV107, 5'-GGCTAGTCCGAAGGTGCAAA-3' for MYC random region 2, AP21, 5’-CTGCCCTAC-TTGTGATGTGG-3’, AP22, 5’-GATGGATGAGTGTGCGTTCT-3’ for RAG2, MN91, 5'-GAA-GCTCTCTTGCACCG-3', SKS10, 5'-CAAGGATCCGCCAACAGCGGCTCCTGGC-3' for HOX11 region II. Same conditions and primers were also used for semiquantitative PCR using γ-irradiated genomic DNA. The additional primers used for semiquantitative PCR were AP1, 5'-GCTGATGGTCAGAAGCCAGT-3', AP2, 5'-GTTGGTCTCCACAGGGTCAG-3', for RAG1, AP3, 5'-AGCCAGGCTTCTCACTGATG-3', AP4, 5'-GGTTGGCAGGCCGGATATTA-3' for RAG2.

Neutral comet assay

Generation of DNA double-strand breaks following irradiation was determined using the comet assay, as described previously (John et al., 2015; Sebastian and Raghavan, 2016). Briefly, cells were harvested post irradiation and washed using PBS. ~10,000 cells were mixed with low melting agarose and spread on an agarose coated glass slide. Cells were lysed overnight at 37^{o}C using neutral lysis buffer (0.5 M EDTA, 2% sarkosyl and 0.5 mg/ml Proteinase K). Slides were then rinsed thoroughly in neutral electrophoresis buffer (90 mM Tris HC (pH 8.0), 90 mM Boric Acid and 2 mM EDTA), and electrophoresed at 12 V for 25 min. Slides were rinsed in double-distilled water, and stained using propidium iodide (2.5 µg/ml for 20 min).

Comets were imaged using an Apotome Fluorescence Microscope (Zeiss, Germany). Comet analyses for the % DNA in tail, tail moment and olive moment were performed using the CometScore software as described before (John et al., 2015; Sebastian and Raghavan, 2016), and the values were plotted as a scatter plot showing individual cell analysis.

G-quadruplex stabilization using small molecules

HeLa and MCF7 cells (50,000/ml) were treated with TMPyP4 (5 μM) for 5 h followed by 10 Gy irradiation. After recovery periods of 30 min, cells were harvested and processed for immunofluorescence against 53BP1 protein, as described earlier. G-quadruplex stabilization by Pyridostatin was performed by treating cells with the compound (2, 5 μM, 24 h), followed by irradiation (10 Gy). Cells were harvested after 30 min and IF was performed using anti-53BP1. In experiments where neutral comet assay was performed to detect DSBs, cells were harvested immediately and used as described above.

WRN helicase knockdown and overexpression within cells

WRN helicase knockdown (using shRNA plasmid against WRN, TRCN-AAB87, B and C), and overexpression (overexpression vector, pMM290) was performed by using the polyethylenimine method of transfection, as described before (Iyer et al., 2016). In brief, ~ $5x10^5$ lakh cells (Nalm6, and HeLa) were transfected with 10 μg of the plasmid, followed by 24 h (for knockdown) or 36 h (for overexpression) incubation at 37^{o}C. Cells were harvested and WRN protein levels were assessed using western blotting. For assessing the effect of radiation on these samples, cells were irradiated (10 Gy), allowed to recover for 30 minutes (or harvested immediately in case of comet assay) and was subjected to either immunofluorescence for detection of 53BP1 foci or neutral comet assay, as described above. In case of the samples where WRN knockdown was done followed by overexpression, cells were first transfected with shRNA (37^{o}C for 24 h) followed by transfection with overexpression construct, pMM290 (37^{o}C for 36 h) and WRN expression was evaluated.

Dataset for analysis

The dataset used for the genome wide bioinformatics analysis was downloaded from the NCBI-SRA database. Whole genome sequence read of irradiated GM12878 (10 Gy, 4 h recovery; SRP022845) and CAL51 (5 Gy, 1 h recovery; ERP004219) cells and unirradiated controls were aligned and compared for missing reads.

Alignment, mapping, and visualization of the samples

The reads of the samples were aligned and mapped to the human hg38 reference genome using the alignment tool BOWTIE2, to generate an alignment file in the sam (SAM:

sequence alignment/map) format. Using SAMtools, the sam files were converted to their equivalent binary formats (BAM: binary alignment/map), which is required to upload and visualize the reads in genome viewer. For visualization, the Integrated Genome Viewer (IGV) was used where the samples were loaded as tracks for a visual comparison.

Extracting the nucleotide sequences, GC content and G4 motif number calculation

To extract the damaged sequences present in a stretch of more than 1000 bases, we first found the number of reads passing through every single nucleotide base position in the genome using a tool known as BEDtools suite. Stretches of more than 1000 bases with no reads passing through them were extracted using a AWK: a featured programming language in UNIX based operating systems. The locations of these stretches were extracted and their fasta sequences were obtained, using the BEDtools suite. To visualize the damaged stretches on the chromosome, 1% of these sequences were obtained from every chromosome through shell-scripting commands and represented on a karyogram using an R (scripting language) package called ggbio. The GC content of these sequences were calculated using AWK and the number of G4 motifs were obtained using the online tools Quadbase and Non-B DB.

Estimation of frequency of G4 motifs and occurrence of DNA breaks in different chromosomes

The percentage of DNA damage in every chromosome was determined as follows. The percentage of damaged regions = (the total length of all the damaged regions/ the length of the entire chromosome)*100. Using hclust (R package), the chromosomes were clustered in two distinct groups, viz. the chromosomes with < 15% damage and those with >15%. Analysis of G4 forming motifs in these groups revealed an Inverse correlation between extent of DNA damage and occurrence of G-quadruplex forming motifs, which was determined using Pearson's correlation coefficient. Subsequently, the average number of G4 motifs/damaged region was calculated. Percentage of damage was plotted on x-axis against the number of G4 motifs per damaged region on y-axis.

Distribution of G4s in the damaged and protected promoters and CDS for all the coding genes in the human genome was determined. The annotated human genome (hg38) protein coding gene locations (CDS in the genome) were mapped to all the unprotected regions (stretches of 1000 or more base pairs with no reads) across the entire genome using the BEDtools suite. The number of such mapped regions was obtained, and the percentage of genes with unprotected CDS was calculated using the equation: % unprotected CDS = (number of unprotected regions in the CDS /total number of CDS in the genome)*100. The unprotected

CDS regions were analyzed for the number of G4 forming units. The total number of G4 forming units in the human genome was obtained from a previous study (Kudlicki, 2016) and subsequently the percentage of G4 forming units in the unprotected CDS regions was calculated as follows: % of G4 forming units in the unprotected regions = (number of G4 forming units in the unprotected CDS / total number of G4 forming units in the CDS)*100. A similar pipeline was followed to obtain % of sequences unprotected in the promoter regions and the % of G4 forming units in the promoters.

Statistical analysis

Statistical significance was determined by GraphPad Prism 5 using the Student's *t* test or one way ANOVA test and the obtained values were considered significant if the p value was less than 0.05. Values are expressed as mean ± SEM. Statistical significance was determined by the GraphPad0-QuickCalcs software using the Student's t-test and Mann-Whitney U test and the values obtained were considered significant if the p value was less than 0.05. Besides, Pearson correlation studies were carried out and if the Correlation coefficient value R was less than -0.5, it was considered to be a negative correlation.

SUPPLEMENTARY REFERENCES

Biffi, G., Tannahill, D., McCafferty, J., and Balasubramanian, S. (2013). Quantitative visualization of DNA G-quadruplex structures in human cells. Nat Chem *5*, 182-186.

Bolte, S., and Cordelieres, F.P. (2006). A guided tour into subcellular colocalization analysis in light microscopy. J Microsc *224*, 213-232.

Das, K., Srivastava, M., and Raghavan, S.C. (2016). GNG Motifs Can Replace a GGG Stretch during G-Quadruplex Formation in a Context Dependent Manner. PloS one *11*, e0158794.

Dimitrova, N., Chen, Y.C., Spector, D.L., and de Lange, T. (2008). 53BP1 promotes non-homologous end joining of telomeres by increasing chromatin mobility. Nature *456*, 524-528.

Iyer, D., Vartak, S.V., Mishra, A., Goldsmith, G., Kumar, S., Srivastava, M., Hegde, M., Gopalakrishnan, V., Glenn, M., Velusamy, M*., et al.* (2016). Identification of a novel BCL2-specific inhibitor that binds predominantly to the BH1 domain. The FEBS journal *283*, 3408-3437.

John, F., George, J., Vartak, S.V., Srivastava, M., Hassan, P.A., Aswal, V.K., Karki, S.S., and Raghavan, S.C. (2015). Enhanced efficacy of pluronic copolymer micelle encapsulated SCR7 against cancer cell proliferation. Macromol Biosci *15*, 521-534.

Kudlicki, A.S. (2016). G-Quadruplexes Involving Both Strands of Genomic DNA Are Highly Abundant and Colocalize with Functional Sites in the Human Genome. PloS one *11*, e0146174.

Kumar, T.S., Kari, V., Choudhary, B., Nambiar, M., Akila, T.S., and Raghavan, S.C. (2010). Anti-apoptotic protein BCL2 down-regulates DNA end joining in cancer cells. The Journal of biological chemistry *285*, 32657-32670.

Nambiar, M., Goldsmith, G., Moorthy, B.T., Lieber, M.R., Joshi, M.V., Choudhary, B., Hosur, R.V., and Raghavan, S.C. (2011). Formation of a G-quadruplex at the BCL2 major breakpoint region of the t(14;18) translocation in follicular lymphoma. Nucleic acids research *39*, 936-948.

Nambiar, M., and Raghavan, S.C. (2010). Prevalence and analysis of t(14;18) and t(11;14) chromosomal translocations in healthy Indian population. Annals of hematology *89*, 35-43.

Nambiar, M., and Raghavan, S.C. (2012). Mechanism of fragility at BCL2 gene minor breakpoint cluster region during t(14;18) chromosomal translocation. The Journal of biological chemistry *287*, 8688-8701.
Nambiar, M., Srivastava, M., Gopalakrishnan, V., Sankaran, S.K., and Raghavan, S.C. (2013). G-quadruplex structures formed at the HOX11 breakpoint region contribute to its fragility during t(10;14) translocation in T-cell leukemia. Molecular and cellular biology *33*, 4266-4281.
Raghavan, S.C., Chastain, P., Lee, J.S., Hegde, B.G., Houston, S., Langen, R., Hsieh, C.L., Haworth, I.S., and Lieber, M.R. (2005). Evidence for a triplex DNA conformation at the bcl-2 major breakpoint region of the t(14;18) translocation. The Journal of biological chemistry *280*, 22749-22760.
Raghavan, S.C., Swanson, P.C., Wu, X., Hsieh, C.L., and Lieber, M.R. (2004). A non-B-DNA structure at the Bcl-2 major breakpoint region is cleaved by the RAG complex. Nature *428*, 88-93.
Rustighi, A., Tessari, M.A., Vascotto, F., Sgarra, R., Giancotti, V., and Manfioletti, G. (2002). A polypyrimidine/polypurine tract within the Hmga2 minimal promoter: a common feature of many growth-related genes. Biochemistry *41*, 1229-1240.
Sambrook, J., Fritsch, E.F., and Maniatis, T. (1989). Molecular cloning: a laboratory manual, 2 edn (Cold Spring Harbor, NY, USA: Cold Spring Harbor Laboratory Press).
Schiavone, D., Guilbaud, G., Murat, P., Papadopoulou, C., Sarkies, P., Prioleau, M.N., Balasubramanian, S., and Sale, J.E. (2014). Determinants of G quadruplex-induced epigenetic instability in REV1-deficient cells. The EMBO journal *33*, 2507-2520.
Sebastian, R., and Raghavan, S.C. (2016). Induction of DNA damage and erroneous repair can explain genomic instability caused by endosulfan. Carcinogenesis *37*, 929-940.
Srivastava, M., Nambiar, M., Sharma, S., Karki, S.S., Goldsmith, G., Hegde, M., Kumar, S., Pandey, M., Singh, R.K., Ray, P.*, et al.* (2012). An inhibitor of nonhomologous end-joining abrogates double-strand break repair and impedes cancer progression. Cell *151*, 1474-1487.
Swanson, C., Saintigny, Y., Emond, M.J., and Monnat, R.J., Jr. (2004). The Werner syndrome protein has separable recombination and survival functions. DNA Repair (Amst) *3*, 475-482.
Wu, Q., Gaddis, S.S., MacLeod, M.C., Walborg, E.F., Thames, H.D., DiGiovanni, J., and Vasquez, K.M. (2007). High-affinity triplex-forming oligonucleotide target sequences in mammalian genomes. Molecular carcinogenesis *46*, 15-23.